

Design, Synthesis, and Functional Evaluation of Leukocyte Function Associated Antigen-1 Antagonists in Early and Late Stages of Cancer Development

Eider San Sebastián,[†] Tahl Zimmerman,[‡] Aizpea Zubia,^{†,§} Yosu Vara,[†] Elyette Martin,[⊥] Finton Sirockin,^{||} Annick Dejaegere,[⊥] Roland H. Stote,[⊥] Xabier Lopez,[§] David Pantoja-Uceda,[#] María Valcárcel,^{∞,●} Lorea Mendoza,[∞] Fernando Vidal-Vanaclocha,^{∞,△} Fernando P. Cossío,^{*,§} and Francisco J. Blanco^{*,‡,×}

[†]Ikerchem Ltd., 20009 San Sebastián, Spain

[‡]Structural Biology Unit, CIC bioGUNE, 48160 Derio, Spain

[§]Departamento de Química Orgánica I, Facultad de Química, Universidad del País Vasco/Euskal Herriko Unibertsitatea, 20018 San Sebastián, Spain

^{||}Novartis Institute for Biomedical Research, CH-4002 Basel, Switzerland

[⊥]Integrated Structural Biology Department, Institut de Génétique et de Biologie Moléculaire et Cellulaire, CNRS UMR7104, INSERM U964, 10412 Illkirch, Strasbourg, France

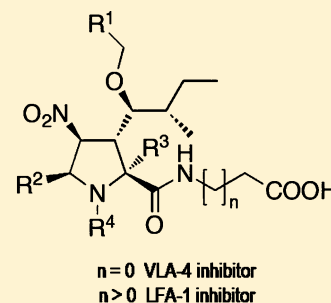
[#]Instituto de Química-Física Rocasolano, CSIC, 28006 Madrid, Spain

[∞]Dominion Pharmakine Ltd., 48160 Derio, Spain

[×]IKERBASQUE, Basque Foundation for Science, 48011 Bilbao, Spain

Supporting Information

ABSTRACT: The integrin leukocyte function associated antigen 1 (LFA-1) binds the intercellular adhesion molecule 1 (ICAM-1) by its α_L -chain inserted domain (I-domain). This interaction plays a key role in cancer and other diseases. We report the structure-based design, small-scale synthesis, and biological activity evaluation of a novel family of LFA-1 antagonists. The design led to the synthesis of a family of highly substituted homochiral pyrrolidines with antiproliferative and antimetastatic activity in a murine model of colon carcinoma, as well as potent antiadhesive properties in several cancer cell lines in the low micromolar range. NMR analysis of their binding to the isolated I-domain shows that they bind to the I-domain allosteric site (IDAS), the binding site of other allosteric LFA-1 inhibitors. These results provide evidence of the potential therapeutic value of a new set of LFA-1 inhibitors, whose further development is facilitated by a synthetic strategy that is versatile and fully stereocontrolled.



INTRODUCTION

LFA-1 (also known as $\alpha_L\beta_2$ or CD11a/CD18) is a heterodimeric protein of the integrin family expressed on the surfaces of all leukocytes and is critical for their antigen-specific responses and homing. The most important natural ligand of LFA-1 is the intercellular adhesion molecule 1 (ICAM-1), which is found on the surfaces of endothelial and epithelial cells, as well as on leukocytes and fibroblasts, and is up-regulated at sites of inflammation.¹ Domain 1 of ICAM-1 interacts with the metal ion dependent adhesion site (MIDAS) of the so-called inserted domain or I-domain of the α_L chain of the integrin (Figure 1). The interaction between ICAM-1 and LFA-1 plays a key role in the pathogenesis of inflammatory and autoimmune disease conditions such as psoriasis, rheumatoid arthritis, and transplant rejection² as well as in the development of various types of cancer metastasis such as gastrointestinal carcinoma,^{3,4} melanoma,^{5,6} lymphoma,^{7,8} and colon carcinoma.⁹ LFA-1 therefore constitutes an attractive therapeutic target

for inhibitors designed to disrupt the LFA-1/ICAM-1 interaction. In this respect, there is strong interest in the design and discovery of low-molecular-weight compounds that could be developed into orally available therapeutics with highly favorable pharmacological properties.

Studies of low-molecular-weight inhibitors of LFA-1 reported to date have revealed the existence of two types of antagonists, one that is allosteric in nature and the other that supposedly acts as a competitive inhibitor, but there is some controversy surrounding the exact binding site.¹⁰ Allosteric inhibitors bind to a hydrophobic cleft between the C-terminal helix and the central β -sheet of the I-domain known as the I-domain allosteric site (IDAS), also known as the lovastatin site (L-site), since this cholesterol-lowering drug was the first allosteric inhibitor of LFA-1 identified.¹¹ Binding to the IDAS is thought

Received: July 5, 2012

Published: January 22, 2013

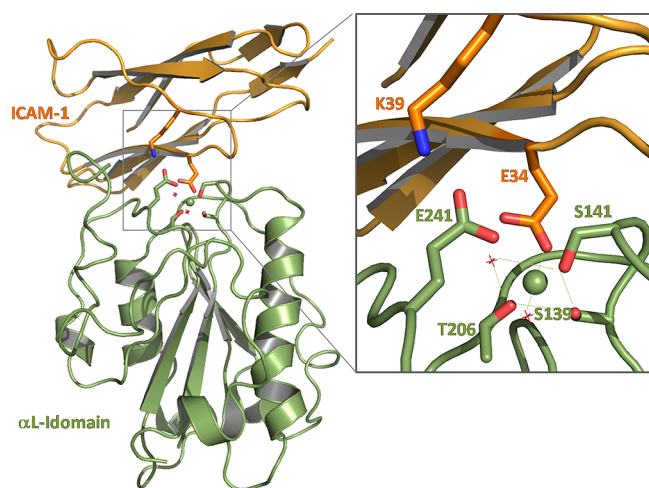


Figure 1. Cartoon representation of the crystal structure (PDB entry 1MQ8) of the complex between the α L I-domain of human LFA-1 (green) and the first three extracellular domains of ICAM-1 (domain 2 is omitted for clarity, and domain 3 was not resolved).¹⁸ The side chains of the residues in both proteins involved in the coordination of the Mg^{2+} cation (represented by a sphere) are shown in sticks with oxygens and nitrogen atoms in red and blue, respectively. Two water molecules coordinating the Mg^{2+} cation are shown as small red crosses. The inset displays the details of the coordination of the Mg^{2+} cation. The side chains of ICAM-1 residue K39 and I-domain residue E241 that form a salt bridge are also shown in sticks. The I-domain present in this structure is a mutant with an engineered disulfide bridge that locks the protein in a conformation with intermediate affinity for ICAM-1.

to stabilize the low-affinity conformation of the I-domain (with a closed MIDAS), preventing its conversion into its high affinity form (open MIDAS) and thereby blocking efficient binding to ICAM-1. Members of the second group were originally described as competitive inhibitors of the α L I-domain/ICAM interaction¹² but were later shown to bind both the α L¹³ and the β 2 integrin chains. These compounds are named α/β I-like allosteric inhibitors.¹⁴ Binding of these inhibitors to the β 2 chain is thought to block the interaction of the α L residue Glu310 with the I-like domain of the β 2 chain, which is structurally similar to the I-domain and contains another MIDAS. The coordination of the α L Glu310 residue with the MIDAS of the β 2 I-like domain is believed to pull the C-terminus of the I-domain and trigger the conformational change into its high affinity form. An inhibitor that blocks this interaction causes the I-domain to remain in its low-affinity conformation.¹⁵ Allosteric inhibitors bind to the IDAS primarily through hydrophobic interactions, while competitive antagonists binding the MIDAS presumably establish additional specific interactions. Highly selective inhibitors are desirable for therapeutic applications to avoid deleterious side effects, but the design of small molecules that compete with ICAM-1 for binding to the MIDAS of the α L I-domain remains a challenging goal.

With the aim of finding novel competitive LFA-1 antagonists we have previously analyzed the geometric and electronic features of the ICAM-1 interaction with the I-domain in both the open and closed conformations of the MIDAS region¹⁶ and studied the most promising chemical motifs for MIDAS binding. Here we describe the rationale for the design, strategy for synthesis, probing of inhibitory activity in vitro and in vivo, in silico optimization, and characterization by nuclear magnetic

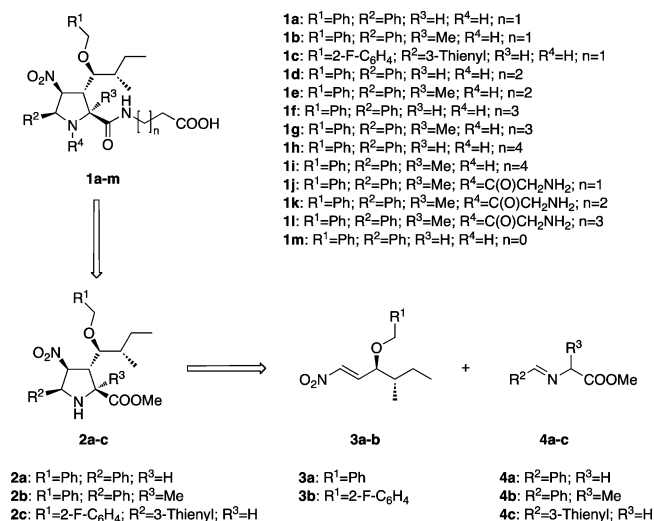
resonance (NMR) of the mechanism of action of a novel family of LFA-1 antagonists.

RESULTS

Design and Chemical Synthesis of LFA-1/ICAM-1 Inhibitors. We have previously described the design of inhibitors of the very late antigen 1/vascular cell adhesion molecule 1 (VLA-4/VCAM-1) interaction on the basis of the geometric and electronic properties of VCAM-1, which led to the generation of highly substituted homochiral pyrrolidines with potent antimetastatic activity in vivo.¹⁷ Because of the high similarity between the three-dimensional structures of VCAM-1 and ICAM-1, we thought that the same approach could be used to generate inhibitors of the LFA-1/ICAM-1 interaction, for which not only the crystal structure of the CAM moiety is known, but also the structure of its complex with the I-domain of LFA-1.¹⁸ Therefore, the design of the first family of LFA-1 antagonists was carried out based on the electronic and geometric features of those residues in ICAM-1 that establish key interactions with the I-domain: Glu34, whose carboxyl group is coordinated with the Mg^{2+} cation at the MIDAS, and Lys39, which forms an ion pair with residue Glu241 in the I-domain (Figure S1A in Supporting Information). In the solvated crystal structure we found that the side chains of residues Glu34 and Lys39 have a high degree of conformational freedom and are surrounded by residues Ile33, Thr35, and Leu54.

Therefore, molecular mimetics of some of these residues were generated (Scheme 1), using highly substituted chiral

Scheme 1. List of Prepared LFA-1 Inhibitors 1a–l and Retrosynthetic Analysis Leading to Intermediates 2a–c, 3a,b, and 4a–c^a



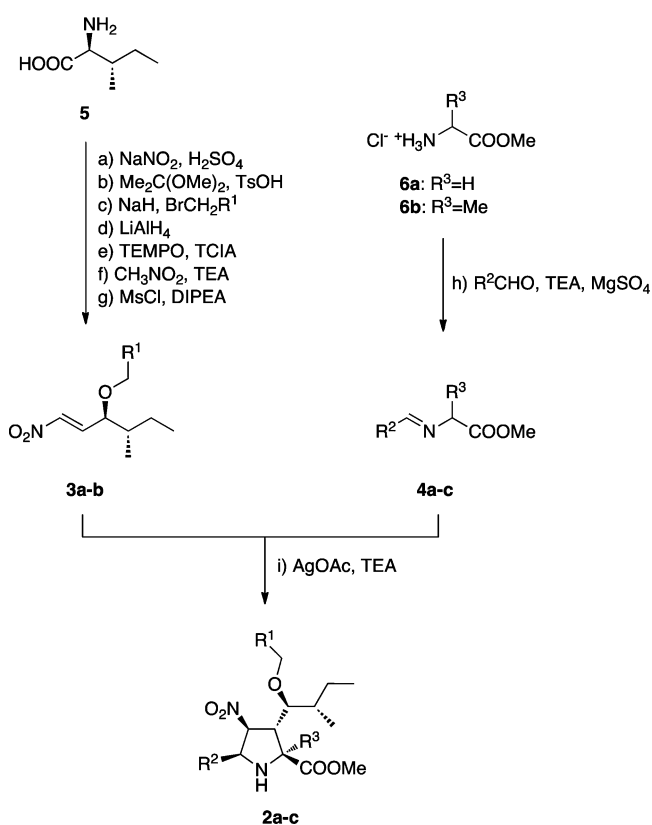
^aSee the Experimental Section and the Supporting Information for further details and compound characterization. Synthesis of VLA-4 inhibitor **1m** was previously described.¹⁷

pyrrolidines as scaffolds. As relevant examples, Figure S1B,C shows the stereoelectronic features of two representative inhibitors. The amino groups of the pyrrolidine ring (**1b**) or the 1-acylamino groups (**1j**) were designed to mimic the amino group of Lys39 of ICAM-1, whereas the carboxyl groups reproduce the negative charge of the Glu34 residue. Since our previous study on the affinity of aliphatic carboxylic acids for

the MIDAS showed that an increase in the length of the alkyl chain beyond $n = 1$ has little effect on the binding,¹⁶ we concluded that this part of the molecule should allow for the elongation of the alkyl chain ($n > 1$; see Scheme 1), if necessary for the better positioning of functional groups. Finally, the alkyl and aryl groups attached to the pyrrolidine ring provide the surrounding environment. The pyrrolidine ring and the four chiral centers restrict conformational freedom. This, in turn, preorganizes the putative inhibitors and therefore decrease the entropy penalty paid for receptor binding.

The chemical synthesis of the novel compounds **1a–i** relies on our previously described method for the synthesis of highly substituted nitroprolines via [3 + 2] cycloadditions between homochiral nitroalkenes **3** and imines **4**,¹⁷ as shown in the retrosynthetic analysis for compound **1** gathered in Scheme 1. Compounds **3a,b** were readily prepared in seven steps from *L*-isoleucine. This preparative sequence involves substitution of the amino group of the starting *L*-amino acid **5** (Scheme 2) by

Scheme 2. Synthesis of Intermediates 2a–c, 3a,b, and 4a–c^a



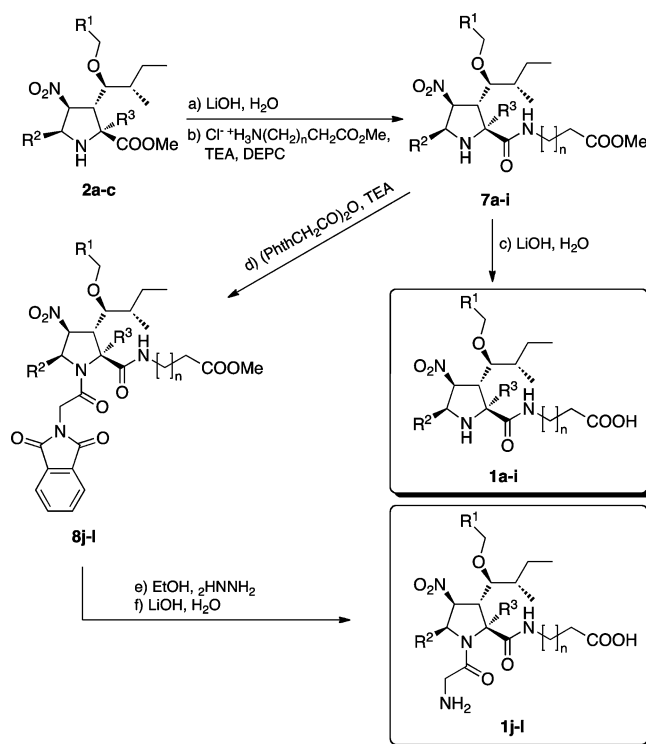
^aUnless otherwise indicated, the substitution patterns are those indicated in Scheme 1. Reagents and conditions: (a) H_2SO_4 1 N, NaNO_2 , 24 h, 0 °C; (b) 2,2-dimethoxypropane, $\text{TsOH} \cdot 2\text{H}_2\text{O}$, MeOH , 24 h, 45 °C; (c) NaH , THF, $\text{R}^1\text{CH}_2\text{Br}$, 72 h, rt; (d) LiAlH_4 , Et_2O , 3 h, rt; (e) TCIA , TEMPO , CH_2Cl_2 , 15 min, rt; (f) CH_3NO_2 , Et_3N , 16 h, rt; (g) MsCl , DIPEA , CH_2Cl_2 , 2 h, –78 °C; (h) R^2CHO , Et_3N , MgSO_4 , CH_2Cl_2 , 16 h, rt; (i) AgOAc , Et_3N , CH_3CN , 5 h, rt.

the hydroxy group with retention of configuration, Williamson coupling with the appropriately substituted benzyl bromide, and nitroaldol reaction before the corresponding elimination reaction.

The starting imines **4a–c** (Schemes 1 and 2) were prepared in one step by condensation between methyl ester hydro-

chlorides **6a,b** and the corresponding aldehyde. Given their instability, these imines were used without further purification. The silver cation mediated [3 + 2] cycloaddition reaction between **4a–c** and the nitroalkenes **3a,b** (Scheme 2) yielded the corresponding pyrrolidines **2a–c**. It is remarkable that in this reaction four stereogenic centers were generated in a single preparative step with complete regio- and stereocontrol. Methyl esters **2a–c** were hydrolyzed and coupled with the corresponding amino acid methyl ester hydrochlorides in the presence of diethyl phosphorocyanidate (Scheme 3) to yield compounds

Scheme 3. Synthesis of Inhibitors 1a–i and 1j–l^a



^aThe substitution patterns are those indicated in Scheme 1. Reagents and conditions: (a) LiOH 1M, DME , 3 h, 0 °C; (b) $\text{HCl} \cdot \text{NH}_2(\text{CH}_2)_n\text{CH}_2\text{COOCH}_3$, Et_3N , diethyl phosphorocyanidate (DEPC), DMF , 16 h, 0 °C to rt; (c) LiOH 1 M, DME , 25 min, 0 °C; (d) *N*-phthaloylglycine anhydride, DMF , Et_3N , 48 h, rt; (e) EtOH , hydrazine, 24 h, 78 °C; (f) LiOH 1 M, DME , 25 min, 0 °C.

7a–i. Simple hydrolysis of these intermediates afforded inhibitors **1a–i** with good yields. In order to prepare analogues of the inhibitors **1a–i** with primary amino residues, compounds **7a–i** were coupled with phthaloylglycine anhydride with moderate yields. Hydrazine deprotection of phthalimidoyl derivatives **8j–l** followed by hydrolysis of the methyl ester moiety resulted in the formation of the desired inhibitors **1j–l**. It is noteworthy that the above-described synthesis of inhibitors is versatile and fully stereocontrolled and uses readily available starting materials. It is therefore well suited for further developments including extensive exploration of the structural space.

Biological Assays with First-Generation Compounds.

In an initial series of cell-based adhesion experiments, compound **1b** emerged as a promising inhibitor of the LFA-1/ICAM-1 interaction and therefore was selected for further testing in *in vitro* and *in vivo* activity assays. As depicted in Figure 2A, preincubation of murine CT26 colon carcinoma

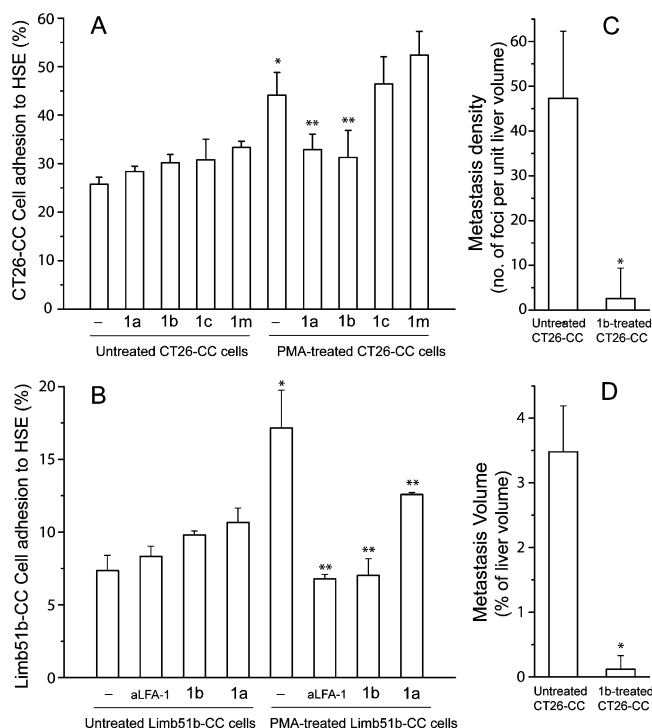


Figure 2. (A) PMA-treated and untreated CT26-CC cell adhesion to HSE cells in the absence and presence of first-generation compounds **1a–c** and the VLA-4 inhibitor **1m**. Statistically significant ($p < 0.05$) differences with respect to untreated (*) or PMA-treated cells (***) are indicated. (B) PMA-treated and untreated Lim51b-CC cell adhesion to HSE cells in the presence and absence of monoclonal antibody aLFA-1, compound **1b**, or compound **1a**. Statistically significant ($p < 0.01$) differences with respect to untreated (*) or PMA-treated cells (***) are indicated. (C) Decrease of metastasis density in mice injected with untreated or compound **1b**-treated CT26-CC cells. Statistically significant ($p < 0.05$) differences with respect to control mice (*) are indicated. (D) Decrease of total metastasis volume in mice injected with untreated or compound **1b**-treated CT26-CC cells. Statistically significant ($p < 0.05$) differences with respect to control mice (*) are indicated.

(CT26-CC) cells with **1a** or **1b** abrogated the increase in CT26-CC cell adhesion to hepatic sinusoidal endothelial (HSE) cells in response to integrin activation by the treatment of the CT26-CC cells with phorbol miristate acetate (PMA), while incubation with compound **1c** did not. Interestingly, the chemically related VLA-4 inhibitor **1m** did not show any inhibitory activity in this assay, indicating that the new family of compounds is specific for the disruption of the LFA-1/ICAM-1 interaction. This conclusion is supported by a reverse experiment (Figure S2A) showing that compound **1b** did not inhibit B16 M cell adhesion to immobilized VCAM-1 (the ligand of VLA-4), providing a cleavage point between the two family of compounds.

We also observed that preincubation of murine Lim51b colon carcinoma (Lim51b-CC) cells with compound **1b** or anti-LFA-1 monoclonal antibody (aLFA-1) abolished the increase in PMA-induced Lim51b-CC cell adhesion to HSE cells and to a larger extent than did incubation with compound **1a** (Figure 2B). Using dose–response data and a simple Hill type equation (Figure S3), the IC_{50} of **1b** was estimated to be in the micromolar range ($IC_{50} \approx 27.6 \mu\text{M}/10^5$ cells). The two colon carcinoma cell lines (CT26 and Lim51b) differ in their rates of growth in vitro and in their ability for metastatic spread

in vivo. Because the CT26 cell line is the most aggressive of the two (displaying a faster growth in vitro and a larger metastatic spread in vivo), further biological assays were conducted using the CT26-CC cells.

Compound **1b** abrogated the PMA-induced CT26 murine colon carcinoma (CT26-CC) cell adhesion to HSE cells, as did the aLFA-1 monoclonal antibody (Figure S2B). Preincubation of B16 melanoma (B16M) cells with either compound **1b** or aLFA-1 abolished the increase in B16M cell adhesion to HSE cells observed in response to the integrin overexpression and activation in HSE cells treated with murine recombinant vascular endothelial growth factor (VEGF; see Figure S2C). Compound **1b** displayed a strong antimetastatic activity in vivo, as seen by the 25-fold reduction in both density and volume of the metastasis produced in mice by the injection of CT26-CC treated with compound **1b** compared to mice receiving untreated cells (Figure 2C,D).

Preincubation of human peripheral blood leukocytes (PBLs) with compound **1b** significantly decreased the PMA-induced PBL adhesion to immobilized human recombinant soluble ICAM-1 (sICAM-1) (Figure 3B), which indicates that the antiadhesive effect of compound **1b** is due to the specific blockade of the interaction between LFA-1 and ICAM-1. In addition, both aLFA-1 and compound **1b** abrogated the increased production of VEGF by B16M cells treated with sICAM-1 and H_2O_2 (Figure S2D).

Structure–Activity Relationship Analysis and Design of Second-Generation Compounds. The cell adhesion results show that compound **1b** is the most potent inhibitor of the LFA-1/ICAM-1 interaction among the first-generation compounds. Compound **1a** is less potent, and compound **1c** is not active. The structure of compound **1a** is very similar to the inactive VLA4 inhibitor **1m** except for a longer chain containing the carboxyl group ($n = 1$; see Scheme 1). This chain lengthening was introduced in the three first-generation compounds to facilitate the coordination of the magnesium cation at the MIDAS, and our results indicate that it is a critical structural feature for their activity. However, compound **1c** does not inhibit CT26-CC cell adhesion, indicating that R^1 and R^2 substituents of a more polar nature than phenyl ones are unfavorable and can override the favorable length of the carboxylic chain. The increase in potency of **1b** relative to **1a** should be due to the increase in size and hydrophobicity conferred by the methyl group as substituent R^3 . A more detailed investigation in 3D space of these issues was assessed by computational methods. Binding of compound **1b** to the MIDAS motif of the high affinity form of the αL I-domain was assessed by virtual docking followed by molecular dynamics (MD) simulation to sample the conformational space of the complex (see the methods section and the Supporting Information for the detailed procedure). The presence or absence of interactions mimicking the coordination of ICAM-1 residue Glu34 to the Mg^{2+} cation and the salt bridge between ICAM-1 residue Lys39 and I-domain residue Glu241 was inspected in snapshots taken at regular time intervals along the MD simulation. As indicated in Figure S4, the interaction of the carboxyl group of the docked **1b** with the Mg^{2+} ion is established and remains stable along the simulation. The distance between the carboxylic oxygen coordinating the cation and the cation is in the range of 3.5–4.2 Å, indicating that the electrostatic interaction is not optimal and suggesting that it could be strengthened by an increase in the chain length. However, the distance between the amino group in compound

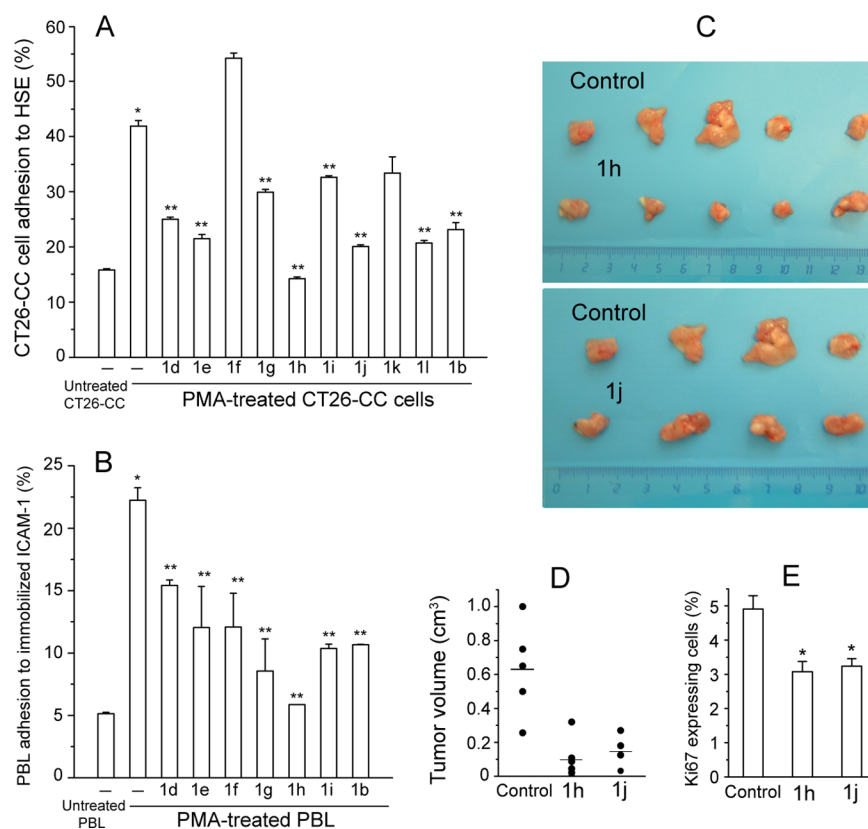


Figure 3. (A) PMA-treated and untreated CT26-CC cell adhesion to HSE cells in the presence and absence of compounds **1d–l** or **1b**. Statistically significant ($p < 0.01$) differences with respect to untreated (*) or PMA-treated cells (**) are indicated. (B) PMA-treated and untreated PBL cell adhesion to immobilized human recombinant ICAM-1 in the presence and absence of compounds **1d–i** or **1b**. Statistically significant ($p < 0.01$) differences with respect to untreated (*) or PMA-treated cells (**) are indicated. (C) Primary tumors induced in mice 15 days after injection of CT26-CC cells and daily treatment with **1h** or **1j**. (D) Volume of the primary tumors shown in (C). (E) Expression levels of protein Ki67 in the same mice primary tumors. Statistically significant ($p < 0.05$) differences with respect to control mice (*) are indicated (see Supporting Information for further details).

1b and Glu241 in the I-domain fluctuates between 9 and 13 Å distances that are too large for a stable salt bridge. Despite the long-range nature of the electrostatic interactions, it can be assumed that no salt bridge is established between these two groups of atoms. These results guided the design of a second generation of inhibitors (Scheme 1, **1d–l**) in which the relative positions of the charged groups were modified to favor the simultaneous formation of the two interactions. This was achieved by elongation of the carboxylic arm of the compounds (**1d–i** in Scheme 1) to provide higher flexibility and therefore greater freedom to bend as needed and by addition of a substituent with a terminal amino group attached to the amino group of the pyrrolidine (**1j–l** in Scheme 1). Elongation of the carboxylic arm in the antagonist is also suggested by the observation that compound **1m**, originally described as a VLA-4 antagonist,¹⁷ does not inhibit LFA-1 (Figure 2A). This compound has an aliphatic carboxylic acid that is a single methylene shorter than **1b** (see Scheme 1). As a first approach to predict the quality of the new structures proposed, the electrostatic potential generated by the two key residues in ICAM-1 (Figure S1A) was compared to the one generated by first-generation compound **1b** (Figure S1B) and second-generation compound **1j** (Figure S1C). Both compounds effectively mimic the spatial distribution and the magnitude of the electrostatic potential generated by the two key residues in ICAM-1. In addition, compound **1j** displays the crevice-like

space between the two electrostatic centers present in the natural ligand (Figure S1A,C).

Biological Assays with Second-Generation Compounds. CT26-CC cell adhesion to HSE cells shows that compounds **1h** and **1j** are stronger inhibitors than first-generation compound **1b** (Figure 3A). Compound **1h** reduced PBL adhesion to immobilized sICAM-1 to basal levels (Figure 3B), indicating that the inhibition is due to the specific blockade of the sICAM-1 dependent adhesion. Compounds **1h** and **1j** were chosen for in vivo assays as representative of the subset of active second-generation compounds with an elongated carboxyl group arm and with an elongated amino group arm, respectively. Compounds **1h** and **1j** decreased the volume of primary tumors in tissues of mice injected with CT26-CC cells by an average of 85% and 77% with respect to the control (Figure 3C,D). They also decreased the expression of the Ki67 antigen by approximately 40% (Figure 3E), a marker of cell proliferation, indicating a reduction of the malignancy or invasive character of primary tumors.¹⁹

Experimental Characterization of Compound Binding and Competition with ICAM-1. To further analyze whether our antagonists inhibit ICAM-1 binding to the LFA-1 I-domain in a competitive manner, their binding site onto the isolated I-domain was mapped by measuring the NMR chemical shift perturbations (CSPs) experienced by the individual I-domain residues upon compound addition. For this purpose, ¹H–¹⁵N HSQC spectra of ¹⁵N enriched I-domain were acquired in the

absence and in the presence of first- and second-generation LFA-1 antagonists.

All the tested LFA-1 antagonists affected the chemical shifts of the same set of I-domain residues (Figure 4A and Figure

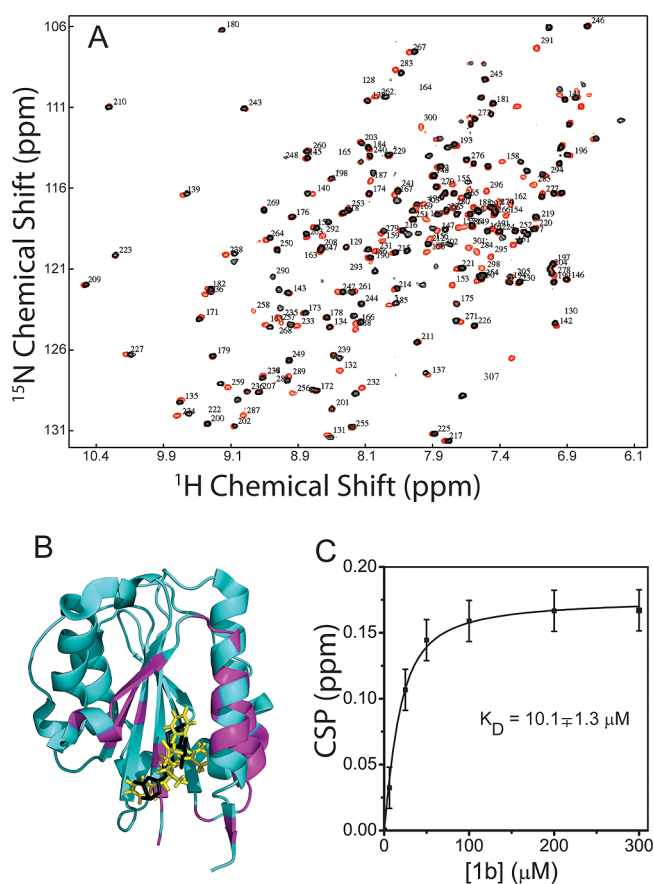


Figure 4. (A) Overlay of the ¹H-¹⁵N HSQC spectrum of the I-domain (50 μM) in the presence (black) or absence (red) of compound **1b** (200 μM) in sodium phosphate buffer pH 7.4 at 22 °C. The numbers beside the signals indicate the corresponding I-domain residue. (B) Cartoon representation of the crystal structure (PDB code 1CQP) of the I-domain (cyan ribbon) in complex with allosteric inhibitor lovastatin (yellow sticks), overlaid with the NMR data guided docked compound **1b** (black sticks). The I-domain in this structure (1ZOP) is the wild type one, with low affinity for ICAM-1. (C) Representation of the CSP experienced by the signal of Thr291 as a function of compound **1b** concentration. The signal of residue Thr291 is located in the upper right corner of the HSQC spectrum shown in panel A. Error bars depict the experimental error of the measurements, and the error in the K_D is the fitting error.

SSA). The residues experiencing the largest CSPs mapped the binding of the compounds to a region encompassing the IDAS (Figure S5B,C), which is the binding site of lovastatin and other allosteric inhibitors.¹¹ To confirm that our compounds bound to the same site as lovastatin, we measured the CSPs caused by lovastatin under our experimental conditions and found the same result (Figure S5D). To examine if the compounds bound to the MIDAS in its open conformation, the high affinity form of the I-domain, we performed the same measurements on a mutant protein locked in the open MIDAS conformation by an engineered disulfide bridge.²⁰ We observed again that residues in the IDAS region were perturbed while the MIDAS residues were not (Figure S5E). The CSPs measured on the mutant I-domain were smaller than those on the wild

type. This observation suggests that the compounds bind to the same region but with a smaller affinity. This is consistent with the absence of a large pocket in the crystal structure of the mutant (PDB code 1MQA).

In all the complexes that were studied by NMR, the CSPs of the MIDAS residues were very small and did not change when the complexes were examined in the presence of the cation chelating agent ethylenediaminetetraacetic acid (EDTA, data not shown). These results confirm that the compounds do not interact with the MIDAS in either the closed or the open conformation of the isolated I-domain. Binding was observed to be highly selective with respect to the αL I-domain subclass, since neither compound **1e** nor lovastatin were found to bind to the I-domain of the integrin α2 chain (Figure S6). Nor did compound **1e** bind to the unrelated B1 domain of protein G (data not shown).

Compound **1b** was docked to the IDAS site of the I-domain using the measured CSPs. The model shows that compound **1b** binds the IDAS in the same place and with an orientation equivalent to that of lovastatin (Figure 4B). A pharmacophore analysis revealed common features in the two structures (Figure S7). In the one of lovastatin bound to the I-domain, there are two hydrophobic features and two hydrogen bond acceptor features. In the structure of compound **1b** docked on the I-domain, these features are also present, although they are not exactly superposable. One of the acceptors in **1b** exhibits a doubled-headed acceptor feature (corresponding to the carboxyl group), although it interacts with the same lysine of the I-domain as lovastatin (K160 and K287 as numbered in 1ZOP and 1CQP, respectively). Compound **1b** also exhibits an additional hydrophobic feature formed by the aromatic group at position R².

The affinity of the binding of selected compounds to the isolated I-domain was determined by titrating the protein with each compound and fitting the measured CSP to a single site binding equilibrium equation (Figure 4C). The values of K_D (\pm fitting error) were 10.1 ± 1.3 and $7.4 \pm 0.8 \mu\text{M}$ for LFA-1 antagonists **1b** and **1e**, respectively, and $12.9 \pm 4.4 \mu\text{M}$ for lovastatin binding to the wild type I-domain. Compound **1b** bound the mutant I-domain locked in the open MIDAS form with $K_D = 81.1 \pm 12.6 \mu\text{M}$. The VLA-4 inhibitor **1m** also bound to the IDAS of the I-domain, although with a 2-fold reduced affinity ($K_D = 19.3 \pm 2.3 \mu\text{M}$). Furthermore, two unrelated compounds (chloramphenicol and ethyl 4,6-dimethoxy-1H-indole-2-carboxylate) used as negative controls also bound to the I-domain and to the same IDAS region as lovastatin and the novel compounds (Figure S8), although they caused much smaller CSPs and thus presumably bind with much smaller affinity.

We next studied the effect of compound binding to the IDAS on the ICAM-1 binding to the I-domain. It has been shown by surface plasmon resonance (SPR) measurements that ICAM-1 binds with very different affinities to the I-domain in the closed or open MIDAS forms ($K_D \approx 1500 \mu\text{M}$ and $K_D \approx 0.15 \mu\text{M}$ for the wild type and mutant I-domains, respectively).¹⁸ SPR measurements show that binding of the mutant I-domain to immobilized ICAM-1 was not abrogated in the presence of saturating amounts of compound **1b** (Figure S9). The binding to the wild type I-domain is too weak to reliably measure the possible inhibition by the compound using SPR, but this can be investigated by NMR. Binding of ICAM-1 reduced the intensity of several I-domain residue signals both in the complex interface (including the MIDAS) and in the IDAS (Figure 5),

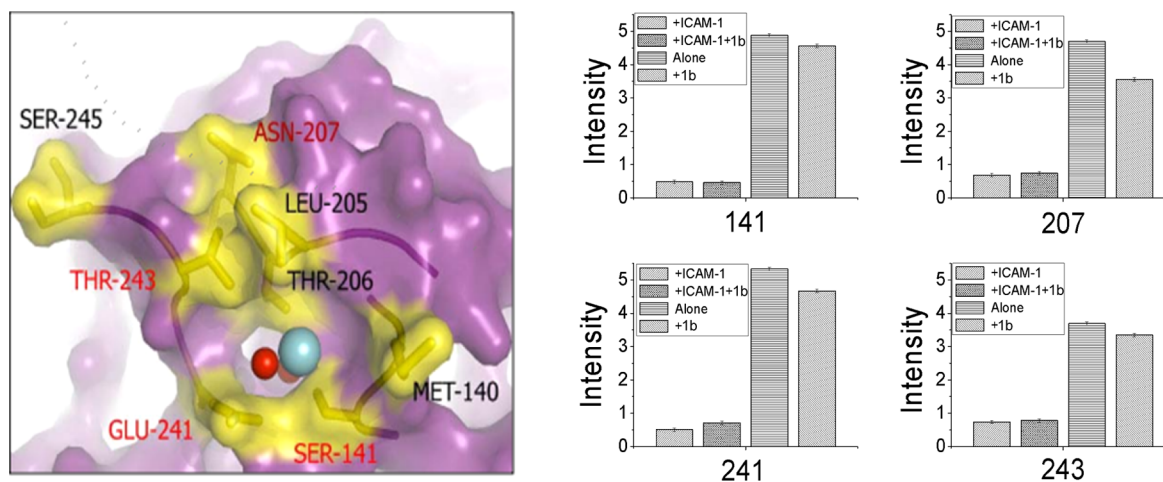


Figure 5. (Left) Representation of the I-domain surface that interacts with ICAM-1 (PDB code 1MQ8). Residues that make direct contacts with ICAM-1 are depicted with yellow sticks and labeled. Residues whose labels are red are those whose cross-peaks recover the least with the addition of compound **1b**. The Mg^{2+} ion and MIDAS site waters are represented by cyan and red spheres, respectively. (Right) Bar graphs of the intensity of the 1H - ^{15}N HSQC signals of the red-labeled residues in the indicated conditions.

which is consistent with the two sites being structurally linked as previously reported.^{21,22} The presence of saturating amounts of the compound provoked a partial recovery in the intensity of some signals in the IDAS region, but little or no recovery was observed for signals of residues known to make direct contacts with ICAM-1, indicating that ICAM-1 binding to the I-domain is not abolished by compound **1b**. These results suggest that ICAM-1 and compound **1b** do not compete for binding to the MIDAS of the isolated I-domain and that compound binding to the IDAS does not block the low-affinity interaction with ICAM-1 in solution. The same conclusion cannot be made with respect to the mutant, since it is locked in its high affinity form by a disulfide bridge.

Binding of our compounds to the I-domain produced CSPs in residues Thr267 and Asp291 (in the $\beta 5$ - $\alpha 6$ and $\beta 6$ - $\alpha 7$ loops, respectively) that, given the large distance between these regions and the IDAS, are likely a consequence of a conformational change induced by compound binding and not of compound binding directly. Indeed, in a previous theoretical study of αL I-domain dynamics, we showed that the dynamics of these two loops were correlated with the IDAS and the $\alpha 7$ helix on one side and the MIDAS on the other.²² Because the two forms of the I-domain must be in equilibrium in solution (with the closed form being the predominant one), these perturbations may report a shift in the equilibrium toward the closed form. Consistent with this hypothesis, we have observed CSPs in the $\beta 5$ - $\alpha 6$ and $\beta 6$ - $\alpha 7$ loop residues of the disulfide bridged mutant on addition of 1,4-dithiothreitol (DTT, which reduces the cystine and unlocks the open conformation of the I-domain presumably shifting the equilibrium toward the closed form; data not shown). We also observed a significant signal broadening in the NMR spectrum of the αL I-domain in residues of these loops and the C-terminus in the presence of ICAM-1 (presumably the consequence of a shift of the conformational equilibrium toward the open form; data not shown). To further characterize the effect of compound binding to the IDAS, we measured the backbone dynamics of the I-domain free and bound to compound **1b** by means of ^{15}N relaxation measurements. The residues in the $\alpha 2$ - $\alpha 3$ (Asp191) and $\beta 5$ - $\alpha 6$ (Thr267) loops, as well as in the C-terminal $\alpha 7$ helix (Glu301, Gln303), are

more dynamic in the picosecond to nanosecond time scale than the rest of the molecule, as is also the N-terminal residue (Figure S10). The relatively flexible character of the $\alpha 2$ - $\alpha 3$ linker and the C-terminal helix in the absence of compound, is consistent with heteronuclear Overhauser effect (NOE) data of the I-domain R189W mutant.²³ In the presence of saturating amounts of compound **1b**, signal broadening made impossible an unambiguous assignment of certain signals and caused an increase in the error of the order parameters in others. Consequently, a comparison of the two sets of parameters for the C-terminal helix was inconclusive. Nevertheless, the average $^{15}N\{^1H\}$ NOE values in this helix change from 0.761 ± 0.016 to 0.822 ± 0.032 (Figure S11), which suggests an increased rigidity in the presence of compound **1b** and that the I-domain is stabilized in its low-affinity closed form. Interestingly, a rigidification of the C-terminal residues of the I-domain upon binding to lovastatin can also be observed by examining the B-factors in the corresponding crystallographic structures (1ZOP and 1CQP, respectively).

DISCUSSION

The structure-based rational design presented here, and our previous experience with the generation of substituted nitroprolines via [3 + 2] cycloadditions between homochiral nitroalkenes and imines, has allowed us to efficiently synthesize a family of novel and potent LFA-1 antagonists based on highly substituted homochiral pyrrolidines. The synthesis of these inhibitors is versatile, fully stereocontrolled, and uses readily available starting materials. In addition, the molecular size and the features of these inhibitors are compatible with the acceptable values for oral bioavailability.²⁴

The in vitro cell adhesion assays show that the compounds inhibit the intercellular adhesion of different cancer cell types mediated by LFA-1. The most potent compounds display little effect on the basal cell adhesion levels but abolish the increase in adhesion when the cells are treated with PMA or VEGF. The compounds display a strong antiproliferative activity in vivo and provoke a reduction in the expression of the Ki67 antigen by the tumor cells, which indicates a reduction in their invasive character and is consistent with the strong antimetastatic activity shown by compound **1b**. Since this compound reduced

the secretion of VEGF by B16M cells, and VEGF promotes the generation of new blood vessels,^{25,26} this observation suggests that the reduction in metastasis volume is due to an antiangiogenic effect of LFA-1 inhibition by compound **1b**. Interestingly a proangiogenic phenotype of CT-26-CC cells has been reported to be activated via LFA-1-dependent VEGF.²⁷

The compounds, especially **1b**, **1h**, and **1j**, reduce the adhesion of cells to immobilized sICAM-1, indicating that they block the interaction between LFA-1 and ICAM-1, as expected. However, they do not block ICAM-1 binding to the isolated I-domain. Even though they were designed to bind to the MIDAS of the LFA-1 I-domain, they do not when the isolated I-domain is studied in solution. Instead they bind to the IDAS, the site of allosteric inhibitors. These apparently contradictory results could be explained by considering one of the following hypotheses: (i) the compounds are competitive inhibitors and bind the MIDAS of the I-domain in the context of the intact integrin heterodimer but not in the isolated I-domain; (ii) the compounds bind to the IDAS site of the integrin and are allosteric inhibitors of LFA-1; (iii) the compounds act allosterically via binding to a site other than the α L I-domain, possibly the MIDAS of the β 2 I-like domain.

The first hypothesis is supported by the success of the design strategy: the compounds were designed to mimic key features in ICAM-1 for its binding to the MIDAS, and in effect these compounds exhibit LFA-1 antagonist activity in cell based in vitro assays and in vivo. Furthermore, a rational optimization of the first-generation inhibitors resulted in a second generation with more potent compounds. In opposition to this hypothesis is the observation that the compounds do not compete for ICAM-1 binding to the isolated I-domain (neither in its low- or high-affinity forms) and thus argue against a competitive mode of action. Still it is possible that the I-domain exhibits different behavior when isolated than when in the context of the whole integrin. To clarify this issue, it would be necessary to study the inhibitory activity of our compounds against full-length active LFA-1.

The second hypothesis is supported by a mode of binding of our compounds to the I-domain similar to that of the allosteric inhibitor lovastatin. We could not detect inhibition of ICAM-1 weak binding to the isolated I-domain in the presence of our compounds, but this fact does not rule out that they act allosterically. There is evidence that when the I-domain is trapped in its closed form (as IDAS binding inhibitors are thought to do), it retains a basal low affinity for ICAM-1, as seen in a mutant I-domain locked in its closed form by a disulfide bridge.¹⁸ As a consequence, an inhibitory effect would only be observed when a given signal that provokes the downward shift of the C-terminal α 7 helix is blocked by an IDAS site binding compound. Rolling adhesion of cells expressing the isolated wild type I-domain on their membranes to immobilized ICAM-1 is inhibited in the presence of allosteric inhibitors,^{28,29} supporting the model whereby IDAS binding inhibitors block the conformational changes leading to the high-affinity form. Further support for the second hypothesis is found in computational studies showing an increased rigidity in the IDAS and C-terminal helix in the presence of an IDAS binding inhibitor,^{22,30} and our backbone dynamics data show that the C-terminus is rigidified in the presence of the IDAS binding compound **1b**. In addition, the full length LFA-1 with its I-domain locked in its open form by a disulfide bridge is resistant to lovastatin³¹ and the same occurs with the isolated and locked-open I-domain expressed on the cell surface.³²

Consistent with these results, our compound **1b** does not disrupt the binding of ICAM-1 to the I-domain locked in the open form by a disulfide bridge. However, it looks as if any small hydrophobic molecules may bind the I-domain IDAS in solution, which raises the question of whether binding of a compound to the promiscuous IDAS really means that it blocks the conformational change to the high-affinity I-domain form. Two considerations suggest that this is not the case for any compound. First, the binding affinity is much smaller for the two unrelated compounds studied here than for our compounds and lovastatin. Second, even minor differences in compound structure affect compound activity, as evidenced by pravastatin, a far less effective inhibitor and weaker binder of the I-domain than lovastatin. The only difference between pravastatin and lovastatin is a hydroxyl group in place of a methyl.³³ So while a variety of compounds have the potential to bind the IDAS, not all have the correct structure for high-affinity binding to the IDAS or for inhibition of the LFA-1/ICAM-1 interaction. To confirm that the mechanism of action of our compounds is purely allosteric, we would need to show that binding to the IDAS leads to inhibition of ICAM-1 binding. However, we cannot observe inhibition of the I-domain in its closed form, and it is impossible to observe allosteric inhibition with the disulfide-bridged active form. Again, the isolated I-domain is not a good model for binding studies with ICAM-1.

The third hypothesis is suggested by the structural similarity between the MIDAS of the I-domain and of the I-like-domain, as well as by the observation that while some of the α/β I-like allosteric inhibitors¹⁴ were designed to be competitive ones,¹² they did not compete with ICAM-1 binding to the isolated I-domain.¹³ Further research on their mechanism of action showed mixed results regarding binding to the I-like-domain¹⁴ or the I-domain¹³ in assays with soluble extracellular domains or with deletion mutants of the integrin heterodimer, respectively. We, however, have no evidence that our compounds act in this way; rather they appear to bind to the IDAS of the isolated I-domain. This is in contrast to what is observed with the α/β I-like allosteric inhibitor XVA143;³⁴ therefore, this third possibility is highly unlikely.

The binding sites of known LFA-1 antagonists have generally been determined by high resolution studies (such as NMR) on the isolated I-domain or by low resolution ones (such as epitope mapping with antibodies) with deletion mutants or the full length integrin. Both experimental approaches have their limitations and may, in the end, yield apparently contradictory results for a system as complex as LFA-1, which contains two multidomain chains, many points of conformational change, and many ion binding sites. Therefore, it may be imprudent to rely only on the isolated I-domain for the study and design of LFA-1 inhibitors, as we and others have done.

CONCLUSION

We have designed a novel family of LFA-1 antagonists that can be synthesized from readily available starting materials. Some of these compounds display potent antiadhesive, antimetastatic, and antiproliferative properties in the low micromolar range in in vitro and in vivo assays. Although these inhibitors were designed to be competitive, they bind to the allosteric site of the isolated α L I-domain. However, neither an allosteric nor a competitive mechanism of action can yet be discerned in the context of the full integrin. The synthetic strategy is versatile and fully stereocontrolled and therefore well suited for further

developments including extensive exploration of the structural space.

EXPERIMENTAL SECTION

Chemical Reagents and Compound Characterization Methods. All starting materials and reagents were purchased from Sigma-Aldrich and used without further purification. Melting points of solid compounds were determined on a Büchi B-540 apparatus and are uncorrected. No melting points are reported for oily compounds. Determination of the purity of tested compounds was performed by combustion analysis (C, H, N) carried out on a Leco CHNS-932 elemental analyzer calibrated with sulfamethazine. The results confirmed a $\geq 95\%$ purity. Merck silica gel 60F-254 plates were used for analytical TLC. NMR spectra were measured in CDCl_3 and $\text{DMSO}-d_6$ on Varian Gemini 200, Bruker Avance 300, and Bruker Avance 500 spectrometers. Chemical shifts (δ) are expressed in ppm and coupling constants (J) in hertz. IR spectra were recorded in a Perkin-Elmer 1600 series FTIR spectrometer connected to a PC using KBr disks. Optical rotations were measured on a Perkin-Elmer 243B polarimeter.

Synthesis of Compounds 7a–i. The corresponding pyrrolidine methyl ester 2a–c (5.0 mmol) was dissolved in DME (25 mL) and cooled to 0 °C. LiOH, 1 N aqueous solution (15 mL), was added dropwise, and the progress of the reaction was monitored by TLC. After completion of the reaction, citric acid, 10% aqueous solution (15 mL, pH \approx 6), was added. The resulting solution was extracted with CH_2Cl_2 (3 \times 20 mL), and the combined organic fractions were dried and evaporated. The crude product was triturated in Et_2O , yielding the corresponding pyrrolidine acid as a white solid. To a round-bottom flask under argon atmosphere, the obtained pyrrolidine 2-carboxylic acid (1 mmol) and the appropriate aliphatic ϵ -amino ester (1 mmol) in 2.5 mL of anhydrous DMF were introduced, and the mixture was cooled with an ice/water bath. DECP (0.18 mL, 1.2 mmol) in 0.5 mL of DMF and TEA (0.29 mL, 2.05 mmol) were added dropwise, and the resulting mixture was stirred at room temperature for 16 h. Then AcOEt (100 mL) and toluene (100 mL) were added, and the organic solution was washed with 50 mL fractions of H_2O , $\text{Na}_2\text{S}_2\text{O}_3$, 1 N aqueous solution, H_2O , NaHCO_3 saturated aqueous solution, and NaCl saturated aqueous solution, dried (Na_2SO_4), and evaporated. The crude mixture was purified by flash chromatography (ethyl acetate/hexanes). The characterization of these intermediate compounds can be found in the Supporting Information.

Synthesis and Characterization of Compounds 1a–i. The corresponding compound 7 (1.0 mmol) was dissolved in DME (5 mL) and cooled to 0 °C. LiOH, 1 N aqueous solution (3 mL), was added dropwise, and the progress of the reaction was monitored by TLC. After completion of the reaction, citric acid, 10% aqueous solution (3 mL, pH \approx 6), was added. The resulting solution was extracted with CH_2Cl_2 (3 \times 4 mL), and the combined organic fractions were dried and evaporated. The crude product was triturated in Et_2O , yielding the corresponding product 1 as a white solid.

{(2S,3R,4S,5S)-3-[(1S)-1-Benzyloxy-2-methylbutyl]-4-nitro-5-phenyl}prolyl- β -alanine, 1a. 98% yield; IR (KBr, cm^{-1}) 3372, 3331, 1728, 1635, 1549, 1365; ^1H NMR (δ ppm, J Hz, CDCl_3) 7.73 (t_b , 1H, $J = 4.9$), 7.38–7.19 (m, 10H), 6.11 (s_b , 2H), 5.35 (dt, 1H, $J = 5.9$, $J' = 1.4$), 4.74 (d, 1H, $J = 11.1$), 4.49 (d, 1H, $J = 6.6$), 4.47 (d, 1H, $J = 11.1$), 3.73 (d, 1H, $J = 7.4$), 3.64 (d, 1H, $J = 5.9$), 3.59–3.42 (m, 2H), 3.15 (d_b , 1H, $J = 5.1$), 2.60 (t, 2H, $J = 5.1$), 1.92–1.78 (m, 1H), 1.59–1.37 (m, 1H), 1.30–1.06 (m, 1H), 0.99–0.83 (m, 6H); ^{13}C NMR (δ ppm, CDCl_3) 175.8, 172.3, 138.0, 134.7, 128.4, 127.7, 126.4, 90.8, 82.5, 72.9, 66.9, 63.6, 50.2, 37.1, 34.6, 33.6, 25.8, 14.3, 11.6; mp 140–141 °C; $[\alpha]_D^{25} + 63.23$ (c 0.99, CH_2Cl_2). Anal. Calcd for $\text{C}_{26}\text{H}_{33}\text{O}_6\text{N}_3$: C, 64.57; H, 6.89; N, 8.69. Found: C, 64.05; H, 6.97; N, 8.62.

{(2S,3R,4S,5S)-3-[(1S)-1-Benzyloxy-2-methylbutyl]-2-methyl-4-nitro-5-phenyl}prolyl- β -alanine, 1b. 93% yield; IR (KBr, cm^{-1}) 3372, 3316, 1729, 1663, 1555, 1372; ^1H NMR (δ ppm, J Hz, CDCl_3) 8.25 (t_b , 1H, $J = 6.2$), 7.38–7.25 (m, 12H), 5.40 (dd, 1H, $J = 6.5$, $J' = 2.5$), 4.69 (d, 1H, $J = 6.5$), 4.67 (d, 1H, $J = 11.1$), 4.39 (d, 1H, $J = 11.3$), 3.81 (d, 1H, $J = 3.9$), 3.65–3.49 (m, 2H), 3.07 (s, 1H), 2.59 (t_b , 2H, $J = 5.5$), 2.08–1.81 (m, 1H), 1.52 (s, 3H), 1.38–1.20 (m, 1H), 1.13–

0.99 (m, 1H), 0.91 (t, 3H, $J = 6.9$), 0.74 (d, 3H, $J = 6.8$); ^{13}C NMR (δ ppm, CDCl_3) 175.9, 138.3, 135.7, 128.7, 128.4, 127.6, 127.3, 126.9, 91.5, 79.7, 70.3, 66.2, 65.0, 50.2, 35.9, 34.7, 34.3, 26.2, 19.5, 13.3, 12.0; mp 104–105 °C; $[\alpha]_D^{25} + 13.23$ (c 0.94, CH_2Cl_2). Anal. Calcd for $\text{C}_{27}\text{H}_{35}\text{O}_6\text{N}_3$: C, 65.16; H, 7.10; N, 8.45. Found: C, 64.59; H, 7.12; N, 8.56.

{(2S,3R,4S,5S)-3-[(1S)-1-(2-Fluorobenzyloxy)-2-methylbutyl]-4-nitro-5-(3-thienyl)prolyl- β -alanine, 1c. 95% yield; IR (KBr, cm^{-1}) 3372, 3332, 1726, 1673, 1552, 1358, 1232; ^1H NMR (δ ppm, J Hz, CDCl_3) 7.83 (t_b , 1H, $J = 5.3$), 7.39–6.90 (m, 7H), 6.31 (s_b , 2H), 5.29 (d_b , 1H, $J = 6.0$), 4.69 (d, 1H, $J = 11.1$), 4.59–4.54 (m, 2H), 3.77 (d, 1H, $J = 7.3$), 3.70–3.46 (m, 3H), 3.18 (d_b , 1H, $J = 6.5$), 2.58 (t_b , 2H, $J = 5.8$), 1.94–1.71 (m, 1H), 1.63–1.38 (m, 1H), 1.31–1.06 (m, 1H), 0.96–0.83 (m, 6H); ^{13}C NMR (δ ppm, CDCl_3) 176.2, 171.6, 163.3, 158.4, 135.6, 130.3, 130.2, 130.0, 129.8, 126.2, 125.8, 124.2, 124.1, 122.7, 115.6, 115.2, 90.3, 82.8, 67.2, 67.1, 63.8, 63.7, 50.4, 37.3, 34.7, 33.7, 25.8, 14.4, 11.6; mp 113–114 °C; $[\alpha]_D^{25} + 63.55$ (c 1.1, CH_2Cl_2). Anal. Calcd for $\text{C}_{24}\text{H}_{30}\text{O}_6\text{N}_3\text{FS}$: C, 56.78; H, 5.97; N, 8.28. Found: C, 56.36; H, 5.97; N, 8.21.

4-[(2S,3R,4S,5S)-3-[(1S,2S)-1-(Benzyloxy)-2-methylbutyl]-4-nitro-5-phenylpyrrolidine-2-carboxamido]butanoic Acid, 1d. 68% yield; IR (KBr, cm^{-1}) 3397, 1733, 1653, 1552, 1362; ^1H NMR (δ ppm, J Hz, CDCl_3) 7.43–7.35 (m, 5H), 7.34–7.29 (m, 6H), 5.36 (dd, 1H, $J = 6.6$, $J' = 2.2$), 4.79 (d, 1H, $J = 11.4$), 4.60 (d, 1H, $J = 6.6$), 4.55 (d, 1H, $J = 11.4$), 3.78 (d, 1H, $J = 5.9$), 3.71 (d, 1H, $J = 7.4$), 3.51–3.44 (m, 1H), 3.40–3.34 (m, 1H), 3.07 (d_b , 1H, $J = 7.3$), 2.42 (dt, 2H, $J = 7.1$, $J' = 2.4$), 1.95–1.89 (m, 2H), 1.88–1.81 (m, 1H), 1.54–1.46 (m, 1H), 1.36–1.30 (m, 1H), 1.22–1.13 (m, 1H), 0.94 (t, 3H, $J = 7.4$), 0.87 (d, 3H, $J = 6.9$); ^{13}C NMR (δ ppm, CDCl_3) 176.7, 173.1, 138.3, 135.1, 128.8, 128.6, 128.4, 127.9, 127.6, 126.7, 91.0, 82.8, 73.2, 67.1, 63.9, 50.5, 38.4, 37.3, 31.3, 26.1, 24.9, 14.5, 11.7; $[\alpha]_D^{25} + 25.0$ (c 1.10, CH_2Cl_2). Anal. Calcd for $\text{C}_{27}\text{H}_{35}\text{O}_6\text{N}_3$: C, 65.17; H, 7.09; N, 8.44. Found: C, 65.03; H, 7.11; N, 8.40.

4-[(2S,3R,4S,5S)-3-[(2S)-1-(Benzyloxy)-2-methylbutyl]-2-methyl-4-nitro-5-phenylpyrrolidine-2-carboxamido]butanoic Acid, 1e. 71% yield; IR (KBr, cm^{-1}) 3387, 3337, 1743, 1663, 1552, 1364; ^1H NMR (δ ppm, J Hz, CDCl_3) 7.98 (t_b , 1H, $J = 5.9$), 7.42–7.29 (m, 10H), 5.47 (dd, 1H, $J = 6.7$, $J' = 2.7$), 4.77 (d, 1H, $J = 6.7$), 4.72 (d, 1H, $J = 11.1$), 4.44 (d, 1H, $J = 11.1$), 3.87 (d, 1H, $J = 4.1$), 3.57–3.50 (m, 1H), 3.37–3.31 (m, 1H), 3.15 (d, 1H, $J = 2.6$), 2.50–2.43 (m, 2H), 2.01–1.93 (m, 2H), 1.88 (d, 1H, $J = 8.6$), 1.60 (s, 3H), 1.37–1.29 (m, 1H), 1.13–1.04 (m, 1H), 0.95 (t, 3H, $J = 7.3$), 0.79 (d, 3H, $J = 7.0$); ^{13}C NMR (δ ppm, CDCl_3) 176.8, 176.1, 138.3, 135.3, 128.9, 128.6, 128.5, 127.7, 127.3, 126.8, 91.4, 79.8, 70.5, 66.4, 65.2, 50.5, 38.5, 36.0, 29.7, 26.4, 25.0, 19.6, 13.4, 12.0; $[\alpha]_D^{25} + 4.8$ (c 1.10, CH_2Cl_2). Anal. Calcd for $\text{C}_{28}\text{H}_{37}\text{O}_6\text{N}_3$: C, 65.73; H, 7.29; N, 8.21. Found: C, 65.67; H, 7.23; N, 8.26.

5-[(2S,3R,4S,5S)-3-[(2S)-1-(Benzyloxy)-2-methylbutyl]-4-nitro-5-phenylpyrrolidine-2-carboxamido]pentanoic Acid, 1f. 70% yield; IR (KBr, cm^{-1}) 3377, 1723, 1663, 1552, 1377; ^1H NMR (δ ppm, J Hz, CDCl_3) 7.41–7.35 (m, 5H), 7.34–7.28 (m, 6H), 5.36 (dd, 1H, $J = 6.6$, $J' = 2.3$), 4.78 (d, 1H, $J = 11.4$), 4.58 (d, 1H, $J = 6.6$), 4.56 (d, 1H, $J = 11.4$), 3.77 (d, 1H, $J = 5.4$), 3.71 (d, 1H, $J = 7.5$), 3.45–3.38 (m, 1H), 3.35–3.29 (m, 1H), 3.08 (d, 1H, $J = 7.4$), 2.40 (t, 2H, $J = 7.1$), 1.89–1.81 (m, 1H), 1.76–1.70 (m, 2H), 1.68–1.62 (m, 2H), 1.55–1.48 (m, 1H), 1.22–1.13 (m, 1H), 0.95 (t, 3H, $J = 7.4$), 0.87 (d, 3H, $J = 6.9$); ^{13}C NMR (δ ppm, CDCl_3) 177.7, 172.6, 138.3, 135.1, 128.8, 128.6, 128.1, 127.9, 127.6, 126.7, 91.0, 82.8, 73.2, 67.1, 64.0, 50.5, 38.6, 37.3, 33.4, 29.0, 26.1, 21.9, 14.5, 11.7; $[\alpha]_D^{25} + 18.3$ (c 0.70, CH_2Cl_2). Anal. Calcd for $\text{C}_{28}\text{H}_{37}\text{O}_6\text{N}_3$: C, 65.73; H, 7.29; N, 8.21. Found: C, 65.70; H, 7.33; N, 8.20.

5-[(2S,3S,4S,5S)-3-[(2S)-1-(Benzyloxy)-2-methylbutyl]-2-methyl-4-nitro-5-phenylpyrrolidine-2-carboxamido]pentanoic Acid, 1g. 75% yield; IR (KBr, cm^{-1}) 3387, 3322, 1733, 1668, 1552, 1372; ^1H NMR (δ ppm, J Hz, CDCl_3) 7.85 (t_b , 1H, $J = 5.9$), 7.43–7.29 (m, 10H), 5.46 (dd, 1H, $J = 6.8$, $J' = 2.9$), 4.75 (d, 1H, $J = 6.8$), 4.71 (d, 1H, $J = 11.1$), 4.44 (d, 1H, $J = 11.1$), 3.86 (d, 1H, $J = 4.1$), 3.49–3.41 (m, 1H), 3.30–3.23 (m, 1H), 3.13 (d, 1H, $J = 2.7$), 2.42 (t, 2H, $J = 6.9$), 1.99–1.92 (m, 1H), 1.79–1.72 (m, 2H), 1.70–1.63 (m, 2H), 1.58 (s, 3H), 1.36–1.28 (m, 1H), 1.11–1.02 (m, 1H), 0.95 (t, 3H, $J = 7.3$), 0.78 (d, 3H, $J =$

= 6.9); ^{13}C NMR (δ ppm, CDCl_3) 177.9, 175.6, 138.4, 135.6, 128.9, 128.5, 128.4, 127.6, 127.3, 126.9, 91.5, 79.9, 70.4, 66.3, 65.2, 50.5, 38.7, 36.1, 33.4, 29.0, 26.3, 21.9, 19.5, 13.4, 12.0; $[\alpha]_{25}^{\text{D}}$ -3.7 (c 1.60, CH_2Cl_2). Anal. Calcd for $\text{C}_{29}\text{H}_{39}\text{O}_6\text{N}_3$: C, 66.26; H, 7.48; N, 7.99. Found: C, 66.35; H, 7.43; N, 7.97.

6-[(2S,3R,4S,5S)-3-[(2S)-1-(Benzyloxy)-2-methylbutyl]-4-nitro-5-phenylpyrrolidine-2-carboxamido]hexanoic Acid, 1h. 57% yield; IR (KBr, cm^{-1}) 3356, 1698, 1658, 1562, 1380; ^1H NMR (δ ppm, J Hz, CDCl_3) 7.42–7.36 (m, 5H), 7.35–7.31 (m, 5H), 7.25 (t, 1H, $J = 5.6$), 5.37 (dd, 1H, $J = 6.6$, $J' = 2.4$), 4.80 (d, 1H, $J = 11.4$), 4.60 (d, 1H, $J = 6.6$), 4.58 (d, 1H, $J = 11.4$), 3.80 (d, 1H, $J = 6.5$), 3.71 (d, 1H, $J = 7.5$), 3.47–3.41 (m, 1H), 3.32–3.25 (m, 1H), 3.08 (d, 1H, $J = 8.0$), 2.37 (t, 2H, $J = 7.4$), 1.90–1.82 (m, 1H), 1.73–1.67 (m, 2H), 1.65–1.59 (m, 2H), 1.54–1.49 (m, 1H), 1.48–1.42 (m, 2H), 1.23–1.14 (m, 1H), 0.96 (t, 3H, $J = 7.4$), 0.87 (d, 3H, $J = 6.9$); ^{13}C NMR (δ ppm, CDCl_3) 177.9, 172.5, 138.4, 135.3, 128.8, 128.6, 127.8, 127.5, 126.7, 91.0, 82.8, 73.2, 67.1, 64.0, 50.5, 38.8, 37.3, 33.7, 29.2, 26.2, 26.1, 24.3, 14.5, 11.7; mp 105–106 °C; $[\alpha]_{25}^{\text{D}}$ $+22.5$ (c 1.10, CH_2Cl_2). Anal. Calcd for $\text{C}_{29}\text{H}_{39}\text{N}_3\text{O}_6$: C, 66.26; H, 7.48; N, 7.99. Found: C, 66.19; H, 7.50; N, 7.98.

6-[(2S,3R,4S,5S)-3-[(2S)-1-(Benzyloxy)-2-methylbutyl]-2-methyl-4-nitro-5-phenylpyrrolidine-2-carboxamido]hexanoic Acid, 1i. 77% yield; IR (KBr, cm^{-1}) 3366, 3332, 1733, 1653, 1542, 1367; ^1H NMR (δ ppm, J Hz, CDCl_3) 7.83 (t, 1H, $J = 5.9$), 7.49–7.28 (m, 10H), 5.46 (dd, 1H, $J = 6.8$, $J' = 2.9$), 4.75 (d, 1H, $J = 6.5$), 4.71 (d, 1H, $J = 11.0$), 4.44 (d, 1H, $J = 11.1$), 3.86 (d, 1H, $J = 4.0$), 3.56–3.39 (m, 1H), 3.29–3.14 (m, 1H), 3.12 (d, 1H, $J = 2.7$), 2.37 (t, 2H, $J = 7.1$), 2.03–1.86 (m, 1H), 1.77–1.60 (m, 4H), 1.58 (s, 3H), 1.53–1.41 (m, 2H), 1.38–1.24 (m, 2H), 0.94 (t, 3H, $J = 6.8$), 0.77 (d, 3H, $J = 6.9$); ^{13}C NMR (δ ppm, CDCl_3) 178.3, 175.4, 138.4, 135.7, 128.9, 128.5, 128.4, 127.6, 127.3, 126.9, 91.5, 79.8, 70.5, 66.3, 65.1, 50.6, 39.0, 36.0, 33.7, 29.3, 26.3, 26.2, 24.3, 19.5, 13.4, 12.0; $[\alpha]_{25}^{\text{D}}$ $+4.9$ (c 0.60, CH_2Cl_2). Anal. Calcd for $\text{C}_{30}\text{H}_{41}\text{N}_3\text{O}_6$: C, 66.77; H, 7.66; N, 7.79. Found: C, 66.56; H, 7.60; N, 7.75.

Synthesis of Compounds 8j–l. The corresponding compound 7 (1.0 mmol) was dissolved in dry DMF (10 mL), and trifluoroacetic acid (0.77 mL, 10.0 mmol) was added dropwise. The mixture was stirred at room temperature for 5 h. Then, solvents were evaporated under reduced pressure and the resulting salt was dissolved in dry DMF (10 mL) under argon atmosphere. Et_3N (0.22 mL, 1.6 mmol) and *N*-phthaloylglycine anhydride (1.26 g, 3.0 mmol) were added, and the mixture was stirred at room temperature for 48 h. After completion of the reaction, the mixture was partitioned between H_2O (5 mL) and CH_2Cl_2 (5 mL). The organic phase was washed with 5 mL fractions of HCl, 1 N aqueous solution, NaHCO_3 saturated aqueous solution, H_2O , and NaCl saturated aqueous solution, dried (Na_2SO_4), and evaporated. The crude mixture was purified by flash chromatography (ethyl acetate/hexanes, 1:2), yielding the corresponding compound 8. The characterization of these intermediate compounds can be found in the Supporting Information.

Synthesis of Compounds 1j–l. To the corresponding compound 8 (1.0 mmol) dissolved in absolute EtOH (15 mL) hydrazine (0.1 mL) was added dropwise, and the mixture was heated at reflux for 24 h. Then the reaction mixture was allowed to reach room temperature and the precipitate was removed by filtration. The filtrate was evaporated under reduced pressure, and the residue was dissolved in DME (5 mL) and cooled to 0 °C. LiOH, 1 N aqueous solution (3 mL), was added dropwise, and the mixture was stirred at room temperature for 3 h. After completion of the reaction, citric acid, 10% aqueous solution (3 mL, pH \approx 6), was added. The resulting solution was extracted with CH_2Cl_2 (5 \times 4 mL), and the combined organic fractions were dried and evaporated. The crude product was triturated in Et_2O , yielding the corresponding product 1 as a white solid.

[(2S,3R,4S,5S)-1-(2-Aminoacetyl)-3-[(2S)-1-(benzyloxy)-2-methylbutyl]-2-methyl-4-nitro-5-phenylprolylamino]- β -alanine, 1j. 72% yield; IR (KBr, cm^{-1}) 3407, 1718, 1673, 1567, 1382; ^1H NMR (δ ppm, J Hz, $\text{DMSO}-d_6$) 7.96 (t, 1H, $J = 5.5$), 7.93–7.86 (m, 1H), 7.38–7.17 (m, 9H), 5.84 (t, 1H, $J = 10.7$), 5.57 (d, 1H, $J = 7.9$), 4.64 (d, 1H, $J = 11.3$), 4.50 (d, 1H, $J = 11.4$), 3.66 (dd, 1H, $J = 11.7$, $J' = 6.7$), 3.51 (t, 1H, $J = 5.3$), 3.41–3.24 (m, 3H), 2.48–2.33 (m, 3H), 1.59 (s, 3H),

1.50–1.43 (m, 1H), 1.41–1.35 (m, 1H), 1.02–0.94 (m, 1H), 0.84 (d, 3H, $J = 6.8$), 0.78 (t, 3H, $J = 7.3$); ^{13}C NMR (δ ppm, $\text{DMSO}-d_6$) 173.0, 171.4, 137.9, 137.0, 132.5, 128.6, 128.0, 127.6, 127.3, 127.0, 125.0, 87.7, 80.7, 74.2, 67.0, 60.1, 58.8, 48.7, 38.1, 35.7, 33.4, 22.4, 15.9, 11.5; mp 115–116 °C; $[\alpha]_{25}^{\text{D}}$ $+7.9$ (c 0.6, CH_2Cl_2). Anal. Calcd for $\text{C}_{29}\text{H}_{38}\text{N}_4\text{O}_7$: C, 62.80; H, 6.91; N, 10.10. Found: C, 62.66; H, 6.93; N, 10.10.

5-[(2S,3R,4S,5S)-1-(2-Aminoacetyl)-3-[(2S)-1-(benzyloxy)-2-methylbutyl]-2-methyl-4-nitro-5-phenylprolylamino]butanoic Acid, 1k. 80% yield; IR (KBr, cm^{-1}) 3417, 1733, 1668, 1562, 1372; ^1H NMR (δ ppm, J Hz, $\text{DMSO}-d_6$) 8.00 (t, 1H, $J = 4.4$), 7.96–7.90 (m, 1H), 7.39–7.15 (m, 9H), 5.83 (t, 1H, $J = 11.4$), 5.61 (d, 1H, $J = 9.5$), 4.65 (d, 1H, $J = 11.3$), 4.51 (d, 1H, $J = 11.3$), 3.65 (dd, 1H, $J = 11.9$, $J' = 6.8$), 3.53 (t, 1H, $J = 6.4$), 3.46 (d, 1H, $J = 15.6$), 3.26–3.17 (m, 1H), 3.11–3.04 (m, 1H), 2.46 (d, 1H, $J = 16.1$), 2.33–2.21 (m, 2H), 1.80–1.68 (m, 2H), 1.61 (s, 3H), 1.50–1.44 (m, 1H), 1.41–1.36 (m, 1H), 1.03–0.94 (m, 1H), 0.84 (d, 3H, $J = 6.7$), 0.78 (t, 3H, $J = 7.4$); ^{13}C NMR (δ ppm, $\text{DMSO}-d_6$) 174.5, 171.1, 137.9, 136.6, 132.4, 128.6, 128.3, 128.0, 127.6, 127.3, 127.0, 125.0, 87.6, 80.5, 74.2, 67.2, 60.1, 48.8, 41.7, 38.1, 31.6, 24.0, 22.4, 15.8, 11.4; mp 132–133 °C; $[\alpha]_{25}^{\text{D}}$ -12.3 (c 0.75, CH_2Cl_2). Anal. Calcd for $\text{C}_{30}\text{H}_{40}\text{N}_4\text{O}_7$: C, 63.36; H, 7.09; N, 9.85. Found: C, 63.19; H, 7.12; N, 9.84.

6-[(2S,3R,4S,5S)-1-(2-Aminoacetyl)-3-[(2S)-1-(benzyloxy)-2-methylbutyl]-2-methyl-4-nitro-5-phenylprolylamino]pentanoic Acid, 1l. 83% yield; IR (KBr, cm^{-1}) 3446, 1715, 1662, 1559, 1374; ^1H NMR (δ ppm, J Hz, $\text{DMSO}-d_6$) 7.85–7–68 (m, 2H), 7.53 (m, 1H), 7.36–7.19 (m, 9H), 5.71 (m, 1H), 5.53 (d, 1H, $J = 9.4$), 4.63 (d, 1H, $J = 11.4$), 4.54 (d, 1H, $J = 11.4$), 3.70 (dd, 1H, $J = 12.1$, $J' = 6.4$), 3.53 (t, 1H, $J = 6.2$), 3.42 (m, 1H), 3.26–3.17 (m, 1H), 3.11–3.04 (m, 1H), 2.45 (s, 1H), 2.29–2.21 (m, 2H), 1.61 (s, 3H), 1.61–1.53 (m, 4H), 1.52–1.39 (m, 2H), 1.08–0.96 (m, 1H), 0.85 (d, 3H, $J = 6.9$), 0.80 (t, 3H, $J = 7.3$); ^{13}C NMR (δ ppm, $\text{DMSO}-d_6$) 172.0, 168.3, 137.8, 129.6, 129.1, 128.3, 127.6, 127.4, 127.2, 93.6, 80.7, 73.7, 71.3, 66.8, 48.3, 39.4, 37.6, 35.3, 28.6, 23.6, 22.4, 18.1, 16.1, 12.1; mp 112–113 °C; $[\alpha]_{25}^{\text{D}}$ $+31.8$ (c 0.65, acetone). Anal. Calcd for $\text{C}_{31}\text{H}_{42}\text{N}_4\text{O}_7$: C, 63.90; H, 7.27; N, 9.62. Found: C, 63.80; H, 7.20; N, 9.50.

Computational Simulations and Docking. The crystal structure of the complex between the I-domain of LFA-1 (disulfide bridged mutant L161C, F299C) and domains 1–3 of ICAM-1 (PDB entry 1MQ8) was used as the starting structure. Only the first domain of ICAM1, which is bound directly to the I-domain, was retained. This reduced complex (see Figure 1) was prepared for computational study by the following procedure. The energy minimized complex was solvated in a 74 Å \times 74 Å \times 74 Å box of TIP3P water molecules. Bond lengths involving bonds between heavy atoms and hydrogen atoms were constrained using the SHAKE algorithm during the whole process. Periodic boundary conditions were set with the complex fixed, and the water molecules were equilibrated for 20 ps at 300 K. The constraints were removed, and the entire system was again equilibrated for 20 ps. Van der Waals interactions were truncated at a cutoff distance of 12 Å using a switch function. Electrostatic interactions were truncated at 12.5 Å using a shift function. All calculations were done using the CHARMM³⁵ program. Docking of compound 1b to the MIDAS site of the mutant I-domain was done by a Monte Carlo search procedure followed by molecular dynamics simulations (MD) using the CHARMM program. The free energy decomposition analysis was done by the molecular mechanics Poisson–Boltzmann surface area method³⁶ following protocols previously described.³⁷ See Supporting Information for further details.

The model of compound 1b bound to the IDAS site of the I-domain was made with the program HADDOCK.³⁸ The residues of the wild type αL I-domain whose signals had changed in the HSQC spectra in the presence of compound 1b above a threshold of the average plus the experimental error were defined as “active” residues for the docking with this program. One-thousand structures were generated of the compound 1b/I-domain complex using the PDB file 1ZOP as an initial structure for the I-domain. The most energetically favorable docked structure was minimized and subjected to a 3 ns molecular dynamics simulation using the CHARMM 27 program and following the same protocol as that explained above. Then 250 ps of a

stable part of the simulation was subsequently used to calculate an average structure that was used as a model of the complex.

Cloning, Expression, and Purification of the LFA-1 I-Domain.

The clone of the I-domain of the human integrin α L chain (Uniprot code P20701) used here codes for residues 128–307 of the α L chain plus an initial methionine (residue numbering refers to the chain after processing of the N-terminal 25-residue long signal peptide). A synthetic gene of this domain with codons optimized for expression in *E. coli* (Entelechon GmbH) was subcloned into the pET14d expression vector. The high affinity I-domain mutant was produced by introducing mutations K287C and K294C by site-directed mutagenesis, as previously described.²⁰ Both clones were expressed at 37 °C in BL21 (DE3) cells, and purification of the wild type and active forms of the LFA-1 I-domain was performed as described^{18,20} except that a single size-exclusion chromatography on a Superdex75 column (GE Health Care) was used after refolding. Protein purity was evaluated by SDS–PAGE. Identity was confirmed by mass spectrometry, and concentration was measured by absorbance at 280 nm using the extinction coefficients calculated from the amino acid composition. Single (¹⁵N) and double (¹³C,¹⁵N) uniformly labeled samples of the wild type and mutant I-domains were produced by expression in minimal medium containing ¹⁵N-NH₄Cl and both ¹⁵N-NH₄Cl and ¹³C-D-glucose, respectively.

NMR Spectroscopy and Data Analysis. NMR spectra were recorded at 22 °C on a 600 MHz Bruker Avance spectrometer with a TXI cryoprobe, of samples in 10 mM sodium phosphate, pH 7.4, 150 mM NaCl, 1 mM MgCl₂ 3% (v/v), ²H₂O, and 80 μ M 2,2-dimethyl-2-silapentane-5-sulfonic acid (DSS) as an internal chemical shift reference. The assignment of the backbone resonances of the LFA-1 I-domain using triple resonance experiments recorded on ¹³C,¹⁵N labeled I-domain protein samples has already been reported³⁹ and deposited (BMRB code 18941), and the same strategy was used here for the assignment of the mutant I-domain. The solubility in the NMR sample buffer was determined at 22 °C for all the compounds and lovastatin in the absence or presence of 0–10% perdeuterated DMSO, and this information was used in the design of the binding and the titration experiments. The binding site of the compounds was mapped analyzing the CSP of the signals assigned in the ¹H–¹⁵N HSQC spectrum of the I-domain in the presence and absence of compound. All signals whose CSP was larger than the average plus the experimental error were considered to be significantly perturbed by the presence of the added compound. Likewise, those peaks that had broadened to the point of disappearance were considered significantly affected. The dissociation constant K_D of the I-domain complexes with compounds **1b**, **1e**, **1m**, and lovastatin was calculated analyzing the CSPs resulting from changes in the amide signal of the I-domain residue Thr291 upon titration with the corresponding compound. Backbone ¹⁵N relaxation measurements and analysis were performed essentially as described.⁴⁰ Compound **1b** disruption of the LFA-1 I-domain/ICAM-1 interaction was investigated on a 100 μ M ¹⁵N-labeled I-domain sample in PBS plus 10 mM MgSO₄, 3 mM HEPES, 0.01% sodium azide, pH 7.4, prepared with or without 100 μ M D1D2-ICAM-1. This molecule contains the first two extracellular soluble domains of ICAM-1 produced in CHO cells as described.⁴¹ NMR spectra of these samples with or without 320 μ M compound **1b** were recorded (4 h long), and the changes in the intensity of the cross-peaks were measured by volume integration.

Cell Adhesion Assays and in Vivo Tumor Growth Experiments. Quantitative evaluation of in vitro intercellular adhesion was carried out based on previously validated bioassays.⁴² In the absence of signaling events, the integrin in the cell surface is in a state of low affinity for its ICAM-1 ligand (bent heterodimer and closed I-domain).⁴³ Therefore, in the assays, cell adhesion is stimulated by cell treatment with VEGF or with PMA. VEGF increases the expression of the two LFA-1 chains in monocytes.⁴⁴ PMA does not affect LFA-1 expression, conformation, or affinity for soluble ICAM-1 but facilitates the ligand-dependent clustering of the integrins on the cell membrane, thus increasing the avidity of the cells for ICAM-1.⁴⁵ For PBL adhesion to immobilized ICAM-1, the commercial form containing the five extracellular domains (R&D Systems) was used. All the results are

the mean \pm standard deviation (SD) of three separate experiments, each in sextuplicate ($n = 18$).

For the hepatic metastasis assay with compound **1b**, hepatic metastases were produced by the intrasplenic injection of 1.5×10^5 viable CT26-CC cells suspended in 0.1 mL of Hank's balanced salt solution into 6- to 8-week-old anesthetized male BALB/c mice ($n = 10$ per group; three independent experiments). Prior to their inoculation the cells were preincubated for 30 min with or without 10 μ g/mL (20 μ g per 5×10^5 cells) of compound **1b** solubilized with poly(amidoamine) dendrimer generation 3.5 (PAMAM G3.5) at a 4:1 ratio (compound/dendrimer). The rationale for this preincubation time is to evaluate the inhibition of the adhesion of the injected cells to the endothelial cells of the mice as the early event in the process of metastasis. In this way, we do something analogous to the in vitro cell adhesion assays where the CT26-CC cells are incubated for 30 min with the compounds before the adhesion to HSE cells. The duration of 30 min is the same as the preincubation of cells with the anti-LFA1 antibody in the in vitro adhesion assays and comes from established procedures used in analogous cell adhesion assays (with B16 M and HSE cells) as previously described.⁴⁶ The same protocol (30 min preincubation) was used previously to evaluate the antimetastatic activity of VLA-4 inhibitors.¹⁷ Mice were killed by cervical dislocation on the 14th day after the injection of cancer cells. Livers were removed, fixed, and processed for histological analyses. An integrated image analysis system (Olympus Microimage 4.0 capture kit) connected to an Olympus BX51TF microscope was used to quantify the number of foci and their average diameters in serially cut and hematoxylin/eosin stained hepatic tissue sections. Densitometric analysis of digitalized microscopic images was used to distinguish metastatic tissue from normal hepatic tissue. Previously described stereological procedures were employed,⁴² and the following parameters were calculated: the liver metastasis density, which was the number of metastases per 100 mm³ of liver (based on the mean number of foci detected in fifteen 10×10 mm² sections per liver) and the liver metastasis volume (mean percentage of liver volume occupied by metastases).

For the antiproliferative assays of compounds **1h** and **1j**, CT26-CC cells (5×10^5) were subcutaneously injected into BALB/c mice. Mice received daily subcutaneous injections of 2.5 mg/kg compound **1h**/PAMAMG3.5 or compound **1j**/PAMAM G3.5. Primary tumors were removed on day 15, and tumor volume was measured. Expression of Ki67 was scored by immunohistochemistry, counting the number of positively stained cells, and was expressed as a percentage of the total tumor cells counted across 10 randomly selected fields of the section examined under the microscope (average \pm standard deviation).

Differences in average values were evaluated for statistical significance by ANOVA and Bonferroni's or Tamhane's post hoc test for in vitro cell adhesion in vivo assays, respectively.

Further details on methods and materials are given as Supporting Information.

■ ASSOCIATED CONTENT

Supporting Information

Complete chemical characterization of intermediates **2a,b**, **7a–i**, **8j–l**, NMR spectra of the final products **1a–l**, detailed experimental and computational procedures, figures of additional in vitro assays for validation of several of the compounds, figures with additional NMR data on compound binding to the I-domain, and tables with data on the docking studies. This material is available free of charge via the Internet at <http://pubs.acs.org>.

■ AUTHOR INFORMATION

Corresponding Author

*For F.P.C.: phone, 34943015442; e-mail, fp.cossio@ehu.es. For F.J.B.: phone, 34946572521; e-mail, fblanco@cicbiogune.es.

Present Addresses

● Innoprot S.L., 48160 Derio, Spain.

△ Institute of Applied Molecular Medicine, CEU-San Pablo University, 28668 Boadilla del Monte, Spain.

Notes

The authors declare no competing financial interest.

ACKNOWLEDGMENTS

This work was financially supported by the Ministerio de Ciencia y Competitividad (MINECO) Grant CTQ2011-28680 to F.J.B., Grant CTQ2010-16959 and Consolider-Ingenio 2010 CSD2007-00006 to F.P.C., and Grant IT-324-07 from the UPV/EHU (UFI QOSYC 11/22) to F.P.C. We thank J. M. Casanovas, at the CNB-CSIC, Madrid, Spain, for the generous gift of the D1-D2-ICAM-1 sample, and we thank C. González, at the IQFR-CSIC, Madrid, Spain, for help with puckering analysis. The SGI/IZO-SGIker UPV/EHU (supported by the National Program for the Promotion of Human Resources within the National Plan of Scientific Research, Development and Innovations, Fondo Social Europeo MCyT) is gratefully acknowledged for generous allocation of computational resources in Spain. The authors acknowledge support from the University of Strasbourg, the Centre National de la Recherche Scientifique (CNRS), and INSERM. The authors also acknowledge the Institut du Développement et des Ressources en Informatique Scientifique (IDRIS), the Centre Informatique National de l'Enseignement Supérieur (CINES), and the Centre d'Etude du Calcul Parallèle de Strasbourg (Université de Strasbourg) for generous allocations of computer time in France. E.M. was supported by the Ligue Nationale Contre le Cancer. We gratefully acknowledge EGIDE and the Ministère des Affaires Étrangères, France for their support.

DEDICATION

This work is dedicated to Jesús María Rico Rodríguez.

ABBREVIATIONS USED

LFA-1, leukocyte function-associated antigen 1; ICAM-1, intercellular adhesion molecule 1; sICAM-1, soluble intercellular adhesion molecule 1; MIDAS, metal ion dependent adhesion site; IDAS, I-domain allosteric site; NMR, nuclear magnetic resonance; DTT, 1,4-dithiothreitol; NOE, nuclear Overhauser effect; TLC, thin layer chromatography; PDB, Protein Data Bank; MD, molecular dynamics; CHO, Chinese hamster ovary; PMA, phorbol myristate acetate; VEGF, vascular endothelial growth factor; CSP, chemical shift perturbation; PBS, phosphate buffered saline; CC, colon carcinoma; VLA-4, very late antigen 1; VCAM-1, vascular cell adhesion molecule 1; PBL, peripheral blood leukocyte; HSE, hepatic sinusoidal endothelial; BMRB, Biological Magnetic Resonance Data Bank

REFERENCES

(1) Gahmberg, C. G. Leukocyte adhesion: CD11/CD18 integrins and intercellular adhesion molecules. *Curr. Opin. Cell Biol.* **1997**, *9*, 643–650.
 (2) Yonekawa, K.; Harlan, J. M. Targeting leukocyte integrins in human diseases. *J. Leukocyte Biol.* **2005**, *77*, 129–140.
 (3) Yasoshima, T.; Denno, R.; Kawaguchi, S.; Sato, N.; Okada, Y.; Ura, H.; Kikuchi, K.; Hirata, K. Establishment and characterization of human gastric carcinoma lines with high metastatic potential in the liver: changes in integrin expression associated with the ability to

metastasize in the liver of nude mice. *Jpn. J. Cancer Res.* **1996**, *87*, 153–160.

(4) Gulubova, M. V. Expression of cell adhesion molecules, their ligands and tumour necrosis factor alpha in the liver of patients with metastatic gastrointestinal carcinomas. *Histochem. J.* **2002**, *34*, 67–77.

(5) Miele, M. E.; Bennett, C. F.; Miller, B. E.; Welch, D. R. Enhanced metastatic ability of TNF-alpha-treated malignant melanoma cells is reduced by intercellular adhesion molecule-1 (ICAM-1, CD54) antisense oligonucleotides. *Exp. Cell Res.* **1994**, *214*, 231–241.

(6) Wang, H. H.; McIntosh, A. R.; Hasinoff, B. B.; MacNeil, B.; Rector, E.; Nance, D. M.; Orr, F. W. Regulation of B16F1 melanoma cell metastasis by inducible functions of the hepatic microvasculature. *Eur. J. Cancer.* **2002**, *38*, 1261–1270.

(7) Harning, R.; Myers, C.; Merluzzi, V. J. Monoclonal antibodies to lymphocyte function-associated antigen-1 inhibit invasion of human lymphoma and metastasis of murine lymphoma. *Clin. Exp. Metastasis* **1993**, *11*, 337–342.

(8) St-Pierre, Y.; Aoudjit, F.; Lalancette, M.; Potworowski, E. F. Dissemination of T cell lymphoma to target organs: a post-homing event implicating ICAM-1 and matrix metalloproteinases. *Leuk. Lymphoma* **1999**, *34*, 53–61.

(9) Fujisaki, T.; Tanaka, Y.; Fujii, K.; Mine, S.; Saito, K.; Yamada, S.; Yamashita, U.; Irimura, T.; Eto, S. CD44 stimulation induces integrin-mediated adhesion of colon cancer cell lines to endothelial cells by up-regulation of integrins and c-Met and activation of integrins. *Cancer Res.* **1999**, *59*, 4427–4434.

(10) Zimmerman, T.; Blanco, F. J. Inhibitors targeting the LFA-1/ICAM-1 cell-adhesion interaction: design and mechanism of action. *Curr. Pharm. Des.* **2008**, *14*, 2128–2139.

(11) Kallen, J.; Welzenbach, K.; Ramage, P.; Geyl, D.; Kriwacki, R.; Legge, G.; Cottens, S.; Weitz-Schmidt, G.; Hommel, U. Structural basis for LFA-1 inhibition upon lovastatin binding to the CD11a I-domain. *J. Mol. Biol.* **1999**, *292*, 1–9.

(12) Gadek, T. R.; Burdick, D. J.; McDowell, R. S.; Stanley, M. S.; Marsters, J. C., Jr.; Paris, K. J.; Oare, D. A.; Reynolds, M. E.; Ladner, C.; Zioncheck, K. A.; Lee, W. P.; Gribbling, P.; Dennis, M. S.; Skelton, N. J.; Tumas, D. B.; Clark, K. R.; Keating, S. M.; Beresini, M. H.; Tilley, J. W.; Presta, L. G.; Bodary, S. C. Generation of an LFA-1 antagonist by the transfer of the ICAM-1 immunoregulatory epitope to a small molecule. *Science* **2002**, *295*, 1086–1089.

(13) Keating, S. M.; Clark, K. R.; Stefanich, L. D.; Arellano, F.; Edwards, C. P.; Bodary, S. C.; Spencer, S. A.; Gadek, T. R.; Marsters, J. C., Jr.; Beresini, M. H. Competition between intercellular adhesion molecule-1 and a small-molecule antagonist for a common binding site on the alpha subunit of lymphocyte function-associated antigen-1. *Protein Sci.* **2006**, *15*, 290–303.

(14) Shimaoka, M.; Salas, A.; Yang, W.; Weitz-Schmidt, G.; Springer, T. A. Small molecule integrin antagonists that bind to the beta2 subunit I-like domain and activate signals in one direction and block them in the other. *Immunity* **2003**, *19*, 391–402.

(15) Yang, W.; Shimaoka, M.; Chen, J.; Springer, T. A. Activation of integrin beta-subunit I-like domains by one-turn C-terminal alpha-helix deletions. *Proc. Natl. Acad. Sci. U.S.A.* **2004**, *101*, 2333–2338.

(16) San Sebastian, E.; Mercero, J. M.; Stote, R. H.; Dejaegere, A.; Cossio, F. P.; Lopez, X. On the affinity regulation of the metal-ion-dependent adhesion sites in integrins. *J. Am. Chem. Soc.* **2006**, *128*, 3554–3563.

(17) Zubia, A.; Mendoza, L.; Vivanco, S.; Aldaba, E.; Carrascal, T.; Lecea, B.; Arrieta, A.; Zimmerman, T.; Vidal-Vanaclocha, F.; Cossio, F. P. Application of stereocontrolled stepwise [3+2] cycloadditions to the preparation of inhibitors of alpha4beta1-integrin-mediated hepatic melanoma metastasis. *Angew. Chem., Int. Ed.* **2005**, *44*, 2903–2907.

(18) Shimaoka, M.; Xiao, T.; Liu, J. H.; Yang, Y.; Dong, Y.; Jun, C. D.; McCormack, A.; Zhang, R.; Joachimiak, A.; Takagi, J.; Wang, J. H.; Springer, T. A. Structures of the alpha L I domain and its complex with ICAM-1 reveal a shape-shifting pathway for integrin regulation. *Cell* **2003**, *112*, 99–111.

(19) Nagasako, Y.; Misawa, K.; Kohashi, S.; Hasegawa, K.; Okawa, Y.; Sano, H.; Takada, A.; Sato, H. Evaluation of malignancy using Ki-67

labeling index for gastric stromal tumor. *Gastric Cancer* **2003**, *6*, 168–172.

(20) Shimaoka, M.; Lu, C.; Palframan, R. T.; von Andrian, U. H.; McCormack, A.; Takagi, J.; Springer, T. A. Reversibly locking a protein fold in an active conformation with a disulfide bond: integrin alphaL I domains with high affinity and antagonist activity in vivo. *Proc. Natl. Acad. Sci. U.S.A.* **2001**, *98*, 6009–6014.

(21) Huth, J. R.; Olejniczak, E. T.; Mendoza, R.; Liang, H.; Harris, E. A.; Lupher, M. L., Jr.; Wilson, A. E.; Fesik, S. W.; Staunton, D. E. NMR and mutagenesis evidence for an I domain allosteric site that regulates lymphocyte function-associated antigen 1 ligand binding. *Proc. Natl. Acad. Sci. U.S.A.* **2000**, *97*, 5231–5236.

(22) Gaillard, T.; Martin, E.; San Sebastian, E.; Cossio, F. P.; Lopez, X.; Dejaegere, A.; Stote, R. H. Comparative normal mode analysis of LFA-1 integrin I-domains. *J. Mol. Biol.* **2007**, *374*, 231–249.

(23) Legge, G. B.; Kriwacki, R. W.; Chung, J.; Hommel, U.; Ramage, P.; Case, D. A.; Dyson, H. J.; Wright, P. E. NMR solution structure of the inserted domain of human leukocyte function associated antigen-1. *J. Mol. Biol.* **2000**, *295*, 1251–1264.

(24) Lipinski, C. A.; Lombardo, F.; Dominy, B. W.; Feeney, P. J. Experimental and computational approaches to estimate solubility and permeability in drug discovery and development settings. *Adv. Drug. Delivery Rev.* **2001**, *46*, 3–26.

(25) Ferrara, N. Vascular endothelial growth factor: basic science and clinical progress. *Endocr. Rev.* **2004**, *25*, 581–611.

(26) Hicklin, D. J.; Ellis, L. M. Role of the vascular endothelial growth factor pathway in tumor growth and angiogenesis. *J. Clin. Oncol* **2005**, *23*, 1011–1027.

(27) Valcarcel, M.; Arteta, B.; Jauregui-beitia, A.; Lopategi, A.; Martinez, I.; Mendoza, L.; Muruzabal, F. J.; Salado, C.; Vidal-Vanaclocha, F. Three-dimensional growth as multicellular spheroid activates the proangiogenic phenotype of colorectal carcinoma cells via LFA-1-dependent VEGF: implications on hepatic micrometastasis. *J. Transl. Med.* **2008**, *6*, 57.

(28) Salas, A.; Shimaoka, M.; Chen, S.; Carman, C. V.; Springer, T. Transition from rolling to firm adhesion is regulated by the conformation of the I domain of the integrin lymphocyte function-associated antigen-1. *J. Biol. Chem.* **2002**, *277*, 50255–50262.

(29) Salas, A.; Shimaoka, M.; Kogan, A. N.; Harwood, C.; von Andrian, U. H.; Springer, T. A. Rolling adhesion through an extended conformation of integrin alphaLbeta2 and relation to alpha I and beta I-like domain interaction. *Immunity* **2004**, *20*, 393–406.

(30) Nam, K.; Maiorov, V.; Feuston, B.; Kearsley, S. Dynamic control of allosteric antagonism of leukocyte function antigen-1 and intercellular adhesion molecule-1 interaction. *Proteins* **2006**, *64*, 376–384.

(31) Lu, C.; Shimaoka, M.; Zang, Q.; Takagi, J.; Springer, T. A. Locking in alternate conformations of the integrin alphaLbeta2 I domain with disulfide bonds reveals functional relationships among integrin domains. *Proc. Natl. Acad. Sci. U.S.A.* **2001**, *98*, 2393–2398.

(32) Lu, C.; Shimaoka, M.; Ferzly, M.; Oxvig, C.; Takagi, J.; Springer, T. A. An isolated, surface-expressed I domain of the integrin alphaLbeta2 is sufficient for strong adhesive function when locked in the open conformation with a disulfide bond. *Proc. Natl. Acad. Sci. U.S.A.* **2001**, *98*, 2387–2392.

(33) Weitz-Schmidt, G.; Welzenbach, K.; Brinkmann, V.; Kamata, T.; Kallen, J.; Bruns, C.; Cottens, S.; Takada, Y.; Hommel, U. Statins selectively inhibit leukocyte function antigen-1 by binding to a novel regulatory integrin site. *Nat. Med.* **2001**, *7*, 687–692.

(34) Welzenbach, K.; Hommel, U.; Weitz-Schmidt, G. Small molecule inhibitors induce conformational changes in the I domain and the I-like domain of lymphocyte function-associated antigen-1. Molecular insights into integrin inhibition. *J. Biol. Chem.* **2002**, *277*, 10590–10598.

(35) Brooks, B. R.; Bruccoleri, R. E.; Olafson, B. D.; States, D. J.; Swaminathan, S.; Karplus, M. CHARMM: a program for macromolecular energy, minimization, and dynamics calculations. *J. Comput. Chem.* **1983**, *4*, 187–217.

(36) Wang, W.; Kollman, P. A. Free energy calculations on dimer stability of the HIV protease using molecular dynamics and a continuum solvent model. *J. Mol. Biol.* **2000**, *303*, 567–582.

(37) Lafont, V.; Schaefer, M.; Stote, R. H.; Altschuh, D.; Dejaegere, A. Protein–protein recognition and interaction hot spots in an antigen–antibody complex: free energy decomposition identifies “efficient amino acids”. *Proteins* **2007**, *67*, 418–434.

(38) Dominguez, C.; Boelens, R.; Bonvin, A. M. HADDOCK: a protein–protein docking approach based on biochemical or biophysical information. *J. Am. Chem. Soc.* **2003**, *125*, 1731–1737.

(39) Zimmerman, T.; Oyarzabal, J.; Sebastian, E. S.; Majumdar, S.; Tejo, B. A.; Siahaan, T. J.; Blanco, F. J. ICAM-1 peptide inhibitors of T-cell adhesion bind to the allosteric site of LFA-1. An NMR characterization. *Chem. Biol. Drug Des.* **2007**, *70*, 347–53.

(40) Pantoja-Uceda, D.; Arolas, J. L.; Garcia, P.; Lopez-Hernandez, E.; Padro, D.; Aviles, F. X.; Blanco, F. J. The NMR structure and dynamics of the two-domain tick carboxypeptidase inhibitor reveal flexibility in its free form and stiffness upon binding to human carboxypeptidase B. *Biochemistry* **2008**, *47*, 7066–7078.

(41) Casasnova, J. M.; Stehle, T.; Liu, J. H.; Wang, J. H.; Springer, T. A. A dimeric crystal structure for the N-terminal two domains of intercellular adhesion molecule-1. *Proc. Natl. Acad. Sci. U.S.A.* **1998**, *95*, 4134–4139.

(42) Vidal-Vanaclocha, F.; Amezcua, C.; Asumendi, A.; Kaplanski, G.; Dinarello, C. A. Interleukin-1 receptor blockade reduces the number and size of murine B16 melanoma hepatic metastases. *Cancer Res.* **1994**, *54*, 2667–2672.

(43) Carman, C. V.; Springer, T. A. Integrin avidity regulation: are changes in affinity and conformation underemphasized? *Curr. Opin. Cell Biol.* **2003**, *15*, 547–556.

(44) Heil, M.; Clauss, M.; Suzuki, K.; Buschmann, I. R.; Willuweit, A.; Fischer, S.; Schaper, W. Vascular endothelial growth factor (VEGF) stimulates monocyte migration through endothelial monolayers via increased integrin expression. *Eur. J. Cell Biol.* **2000**, *79*, 850–857.

(45) Constantin, G.; Majeed, M.; Giagulli, C.; Piccio, L.; Kim, J. Y.; Butcher, E. C.; Laudanna, C. Chemokines trigger immediate beta2 integrin affinity and mobility changes: differential regulation and roles in lymphocyte arrest under flow. *Immunity* **2000**, *13*, 759–769.

(46) Mendoza, L.; Carrascal, T.; De Luca, M.; Fuentes, A. M.; Salado, C.; Blanco, J.; Vidal-Vanaclocha, F. Hydrogen peroxide mediates vascular cell adhesion molecule-1 expression from interleukin-18-activated hepatic sinusoidal endothelium: implications for circulating cancer cell arrest in the murine liver. *Hepatology* **2001**, *34*, 298–310.